Understanding the Impact of Cycling Parameters on Cell Ageing Using Explainable Machine Learning

Hemanth Neelgund Ramesh

A thesis
submitted in partial fulfillment of the
requirements for the degree of

Master of Science

University of Washington

2024

Committee :
Guozhong Cao
Shijing Sun

Program Authorized to Offer Degree:
Materials Science and Engineering

University of Washington

Abstract

Understanding the Impact of Cycling Parameters
on Cell Ageing Using Explainable Machine Learning

Hemanth Neelgund Ramesh

Chair of the Supervisory Committee :
Guozhong Cao
Materials Science and Engineering

Lithium-ion batteries (LIBs) undergo irreversible and complex aging processes, making it essential to evaluate how different parameters influence their cycle life. While previous studies have examined ageing behavior by changing individual cycling parameters, the cumulative effects of multiple parameters remain largely unexplored. Therefore, in this study, we employ explainable machine learning techniques on 28 LIBs from publicly available data to gain comprehensive understanding about the contribution and interaction of various parameters towards degradation as the battery ages. Our results suggest that in the early stages of battery life (State of Health (SOH) between 1.00 and 0.90), the degradation is sensitive to change in temperature, which is likely due to the abundance of available electrolyte. As the battery ages (SOH between 0.875 and 0.800), charging current emerges as the primary degradation factor. This shift is attributed to the development of the solid electrolyte interphase (SEI) and the subsequent decline in electrolyte quality, which leads to uneven charge density distribution and localized thermal effects, such as Joule heating. Additionally, the charging current and temperature show large interaction effects causing degradation. These findings are

consistent with existing literature regarding changes in degradation mechanisms over the aging period. By offering a qualitative analysis of the differential impact of various parameters on cell aging, our study provides a novel understanding of battery degradation mechanisms. This work lays a solid foundation for future research aimed at extending the cycle life and improving the safety of LIBs using data-driven methods.

Contents

1 Introduction **1**

2 Literature review **4**

3 Methods **10**

3.1 Dataset 10

3.2 Data processing 11

3.3 Machine learning modeling 11

3.4 Model explainability 12

4 Results and Discussion **14**

5 Conclusion **21**

References **23**

A Supplementry **32**

List of Figures

1.1 A plot between cell price and LIB demand over the years. BNEF refers to Bloomberg New Energy Finances. Reproduced with permission from ref [1]. Copyright 2023 Nature. 1

1.2 A plot between cell price and LIB demand over the years. BNEF refers to Bloomberg New Energy Finances. 2

2.1 A schematic figure showing different degradation mechanism within the cell. Reproduced with permission from ref [6]. Copyright 2017 Elsevier. . 4

2.2 A plot showing the increasing complexity of various physics-based models with increase in accuracy relative to data-driven methods. Equivalent circuit model (ECM), single particle model (SPM), P2D and data-driven methods. Reproduced with permission from ref [29]. Copyright 2020 Nature. 5

2.3 A series of plot showing the applications of data-driven methods employed for battery prognosis and diagnosis. Reproduced with permission from ref [42]. Copyright 2024 Nature. 7

2.4 A schematic figure showing SHAP values between cycling parameters and equivalent full cycles (EFC) (top) and SOH metrics (bottom). Reproduced with permission from ref [58]. Copyright 2023 arXiv. 8

3.1 A spider plot comparing various open source datasets. 11

3.2 Schematic graphics showing the methodology of this work. a) Data processing the raw input file into learning dataset. b)Random forest model training. c) Model explainability in terms of feature importance and interactions. 12

4.1 Spearman's rank correlation coefficients for all the cycling parameters from 1.00 to 0.80 SOH. 14

4.2 The calculated p-values for all the cycling parameters from 1.00 to 0.80 SOH. 15

4.3 A combined parity plot for all the SOH subsets. 16

4.4 A stacked bar plot for SHAP based feature importance. 16

4.5 A stacked bar plot for impurity-based feature importance. 17

4.6 A stacked bar plot for permutation-based feature importance. 18

4.7 Influence of cycling parameters on capacity decay. a) The influence of temperature on cycle life of batteries and the orange line represents change in rate of degradation. Reproduced with permission from ref [9]. Copyright 2023 IOP Publishing. b) The influence of charging current on cycle life of batteries and the orange line represents change in rate of degradation. Reproduced with permission from ref [79]. Copyright 2019 Elsevier. . . . 19

4.8 A bar plot for H-statistics based feature interactions. 20

5.1 Schematic illustration showing the summary of our findings 22

A.1 A histogram showing dSOH/dNeq distribution for all the SOH subsets. . 34

A.2 A sample histogram showing cycling conditions (features) distribution for 0.975 SOH. The distribution is same for remaining SOHs. 35

A.3 Spearman's rank correlation coefficient at 1.00 SOH 36

A.4 Spearman's rank correlation coefficient at 0.975 SOH 36

A.5 Spearman's rank correlation coefficient at 0.95 SOH 37

A.6 Spearman's rank correlation coefficient at 0.925 SOH 37

A.7 Spearman's rank correlation coefficient at 0.90 SOH 38

A.8 Spearman's rank correlation coefficient at 0.875 SOH 38

A.9 Spearman's rank correlation coefficient at 0.85 SOH 39

A.10 Spearman's rank correlation coefficient at 0.825 SOH 39

A.11 Spearman's rank correlation coefficient at 0.80 SOH 40

A.12 A comparison of fresh (top) and degraded (bottom) cells due to the effect of temperatures. a) The growth of SEI layer with increase in temperature observed by scanning electron microscopy (SEM) images. Reproduced with permission from ref [11]. Copyright 2014 Elsevier. b) The occurrence of lithium platting at low temperature observed by x-ray computed tomography. Reproduced with permission from ref [9]. Copyright 2023 IOP Publishing. 41

A.13 SEM images showing the early degradation of a cell (lithium platting and particle detachment) with increase in charge/discharge rates. Reproduced with permission from ref [79]. Copyright 2023 Elsevier. 41

A.14 A plot showing the effect of DoD for NMC 18650 cell at 0.5 C discharge and 25 °C. Reproduced with permission from ref [13]. Copyright 2020 IOP Publishing. 42

A.15 A bar plot for H-statistics based feature importance. 42

List of Tables

A.1 A sample dataset for cell 1 32

A.2 A sample subset for all the 28 cells at 0.95 SOH 33

A.3 Compiled evaluation metrics for random forest regression. 40

A.4 Five fold cross validation scores 40

Dedication

To my sister, parents and family.

Your love and support has been a constant source of strength
and inspiration to me. Words fall short to pen down my gratitude.

Acknowledgments

First and foremost, I would like to express my sincere gratitude to my advisors, Prof. Guozhong Cao from Materials Science and Engineering and Dr. Shijing Sun from Mechanical Engineering, for their exceptional guidance, support, and mentorship throughout this project. Prof. Cao's profound knowledge of energy storage materials was instrumental in initiating this project, while Dr. Sun's keen insights into model explainability were essential in developing our novel methodology. I am deeply indebted to them for providing me with invaluable opportunities and unwavering encouragement throughout my academic journey.

Secondly, I extend my sincere gratitude to Prof. Juan Carlos Idrobo from Materials Science and Engineering and Dr. Elif Karatay from Electric Hydrogen for their confidence in me and their support of my research endeavors.

Thirdly, I am grateful to the Sol-Gel research group for the initial brainstorming session and the UW Sun lab for their collaboration and assistance in building machine learning models. I truly enjoyed my time with both groups, and the shared experiences made this journey incredibly rewarding.

Lastly, to friends back in India, Seattle, and Boston, whose unwavering friendship and endless patience in listening to my research ramblings have made this journey infinitely more enjoyable.

I would also like to acknowledge ChatGPT and other related tools for assisting in code debugging and occasional grammar checks.

Chapter 1

Introduction

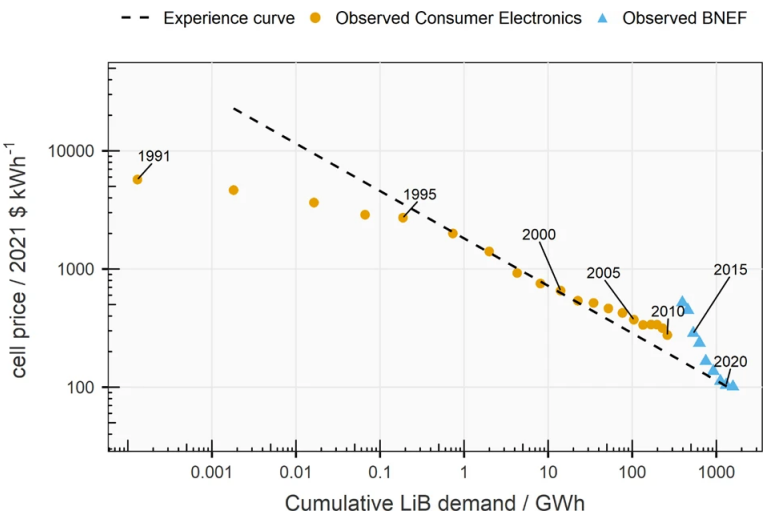

Figure 1.1: A plot between cell price and LIB demand over the years. BNEF refers to Bloomberg New Energy Finances. Reproduced with permission from ref [1]. Copyright 2023 Nature.

Since the past decade, there has been an increasing demand for the production of lithium-ion batteries (LIBs) driven by their applications in electric vehicles and portable electronics. [2] This demand has led to continuous improvements in their performance in terms of energy density, power density, and cycle life. [1, 3] the emergence of large-scale manufacturing facilities, such as gigafactories, has significantly reduced cell costs over the years, as illustrated in Figure 1.1. Despite these advancements, the electrochemical nature of LIBs leads to irreversible ageing throughout their cycle life. [4, 5] This degradation is driven by various physical and cycling parameters that initiate ageing

mechanisms. To better understand this behavior, modeling approaches has been widely used to simulate cell degradation. Among them data-driven algorithms integrated with interpretable models can comprehensively provide insights about the influence of different parameters on degradation. Such knowledge are invaluable for reducing battery replacement costs and accelerating the transition to a sustainable environment. This chapter provides a overview of this thesis by detailing different chapters below.

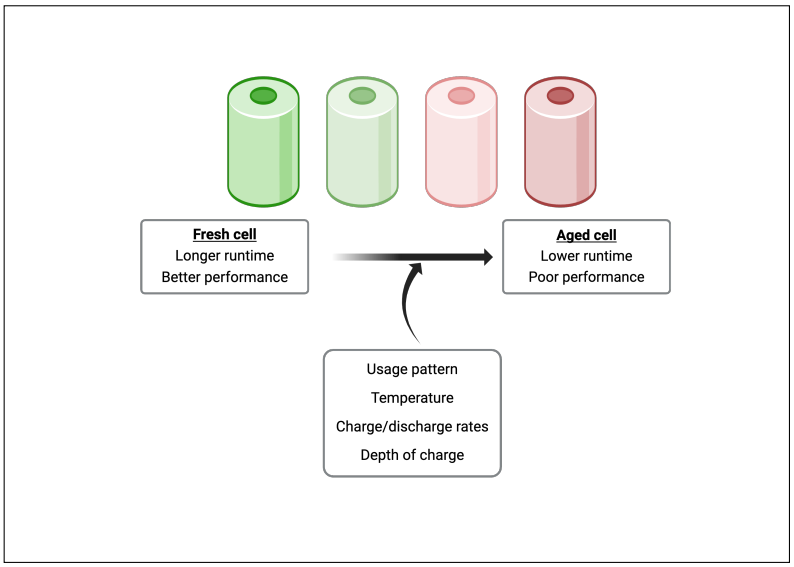

Figure 1.2: A plot between cell price and LIB demand over the years. BNEF refers to Bloomberg New Energy Finances.

In Chapter 2, we conduct a comprehensive literature survey on common degradation mechanisms occurring within battery during ageing. We examine the impact of various parameters on cell ageing. The state of the art modeling techniques, including empirical, physics-based, and data-driven models, are thoroughly reviewed. In addition, we report on interpretable and explainable machine learning (ML) methods applied to battery health prognosis. We also highlight the existing gaps in the literature that has motivated the current study.

In Chapter 3, we outline the methodology employed in this study. We begin with processing the raw data by dividing the large dataset into smaller subsets. These subsets are then introduced as inputs to ML models. Numerous error metrics were calculated to evaluate model fit. The predictions and the trained models are subsequently analyzed using interpretable ML strategies to gain insights into the degradation modes over the cell's ageing process.

Chapter 4 presents the results from our methodology step by step. We first dis-

cuss about various data analysis methods applied to all the subsets prior to ML training. The predictions results are demonstrated using parity plots and multiple metrics showing the fit of the trained model. Additionally, the results from interpretable machine learning are summarized in a stacked bar plot for easier comparison. Based on these learning, we propose a hypothesis and provide relevant supporting literature evidence to see if our hypothesis is valid and makes sense.

Finally, Chapter 5 summarizes the findings from this study and outlines its limitations. We also provide future perspectives on employing interpretable ML as a feedback loop to ensure safe battery operation.

Chapter 2

Literature review

The performance and longevity of batteries are heavily influenced by their cycling conditions and usage. Understanding these mechanisms is crucial for advancing battery innovation. This chapter provides a comprehensive review of the literature on battery degradation, covering various modeling approaches and interpretability and highlighting key findings.

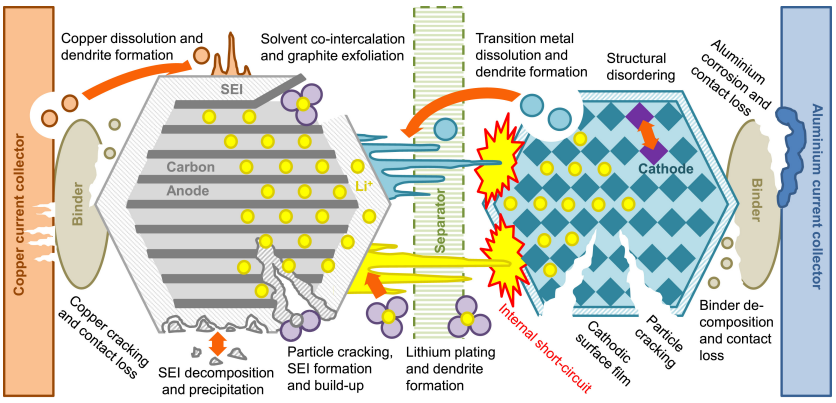

Figure 2.1: A schematic figure showing different degradation mechanism within the cell. Reproduced with permission from ref [6]. Copyright 2017 Elsevier.

The extent and behavior of battery degradation depends on combination of chemical (electrolyte, active material) and physical parameters (usage patterns, temperature, charge/discharge current rates). Several excellent studies have covered the topic of cell ageing and its influencing parameters. [6–17] Figure 2.1 shows various degradation within a cell, which sometimes may occur simultaneously at different length scales. Generally, degradation modes is linked to i) loss of lithium inventory (LLI) and ii) loss

of active material (LAM) in anode and cathode or iii) corrosion of current collectors. [6] For example, electrolyte decomposition forms an interficial layer between electrolyte and electrode, which prevents further decomposition. [18–20] However, over time the interficial layer grows causing increase in internal resistance. During charging/discharging cycles, the electrode materials undergo stress due frequent structural changes which results in mechanical detachment of active material from the electrode. [8, 21, 22] Using X-ray diffraction methods Kondrakov *et al.*, showed that the accelerated ageing is associated to LAM due to anisotropic lattice change. [23] Additionally, other cell components such as current collector and jellyroll tape also contribute to cell degradation via corrosion due to side reaction with electrolyte. [24, 25] Various studies have shown that increasing or decreasing temperature negatively effects battery degradation leading to capacity decay from LLI and LAM. [9,11,26,27] Moreover, fast charging or discharging during abnormal temperature conditions causes serious capacity decay. [14] Laforgue *et al.* conducted a comparative study on the degradation of 18650 cells subjected to temperatures of 23°C and below. [28] From the post-mortem analysis they revealed that, the cell cycled at lower temperatures exhibited severe degradation from lithium plating, active material fracture, jellyroll deformation, and graphite exfoliation. Whereas, cells cycled at room temperature displayed minimal degradation. For the purpose of understanding complex degradation, various modeling techniques have been developed.

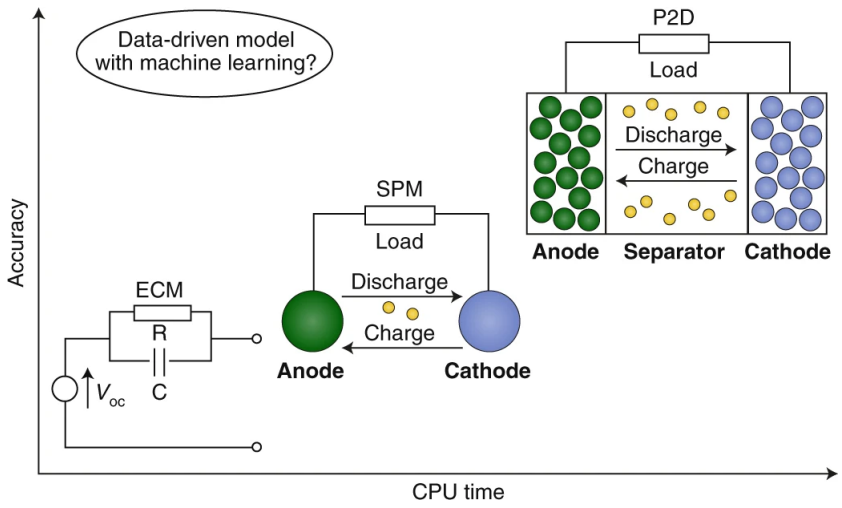

Figure 2.2: A plot showing the increasing complexity of various physics-based models with increase in accuracy relative to data-driven methods. Equivalent circuit model (ECM), single particle model (SPM), P2D and data-driven methods. Reproduced with permission from ref [29]. Copyright 2020 Nature.

Traditional modeling techniques employ both empirical and physics-based models (PBMs) to understand the degradation and to predict cycle life (figure 2.2. [30–33]

Empirical methods rely on experimental data to forecast long-term capacity fade using power laws. [32, 34] Examples of such models include the open circuit voltage model, ampere-hour integral method, and other model-based strategies widely used to estimate the state of charge (SOC). [35] However, these models are often specific to particular chemistries and operating conditions, limiting their generalizability. [29, 36] Moreover, their accuracy is constrained by the extent of parameterization, and they often fail to capture long-range predictions. An improvement to empirical methods is the use of PBMs, which are more robust in providing accurate insights into degradation mechanisms. [32,36] PBMs are based on first-principle approaches that utilize partial differential equations to describe the internal physics and electrochemistry of batteries. A widely used example is the pseudo 2-dimensional (P2D) model developed by Newman and group [37], which simulates lithium-ion dynamics within porous 2D material, providing insights into phenomena like lithium plating. [29, 32] Other underlying mechanisms, such as impedance growth, SEI (solid electrolyte interphase) growth, and active material loss, have also been modeled. [29, 31, 38–40] For instance, von Wald *et al.* used molecular dynamics and density functional theory to model and understand the intercalation of lithium ions through the SEI layer. [41] However, PBM are complex as it involve large number of parameters which can be computationally expensive and requires domain-level expertise. Although, PBM offer some insights into degradation mechanism, they present challenges in terms of chemistry-specific modeling and parameterization to replicate actual cell degradation.

In the recent years, data-driven methods have been extensively explored for battery state prediction such SOH, SOC, remaining useful life (RUL), trajectory of ageing and knee point as shown in figure 2.3. [43–46] Unlike PBM or empirical models, machine learning (ML) models are effective in capturing the non-linear and complex aging behavior of batteries with less computational efforts (figure 2.2). [47, 48] The predictive power of statistical and ML approaches can precisely recognize hidden patterns in large feature spaces. One of the simplest approach is to map the cycle number against discharge capacity to predict the future of degradation and sometimes up to end of life of battery. [49] Many studies have also focused on extracting valuable information from charge discharge time-series data to accurately predict the capacity decay. [50] For example, Severson *et al.*, derived new features from cycling data of first hundred cycles to forecast capacity decay with an error of around 100 cycles. [47] Similarly, history-agnostic methods have also been reported, which uses recent available information from time series data for short and long-term extrapolation. [51] Furthermore, the characteristic features from electrochemical impedance spectroscopy [36, 48] and acoustic time-of-flight [52, 53] are utilized

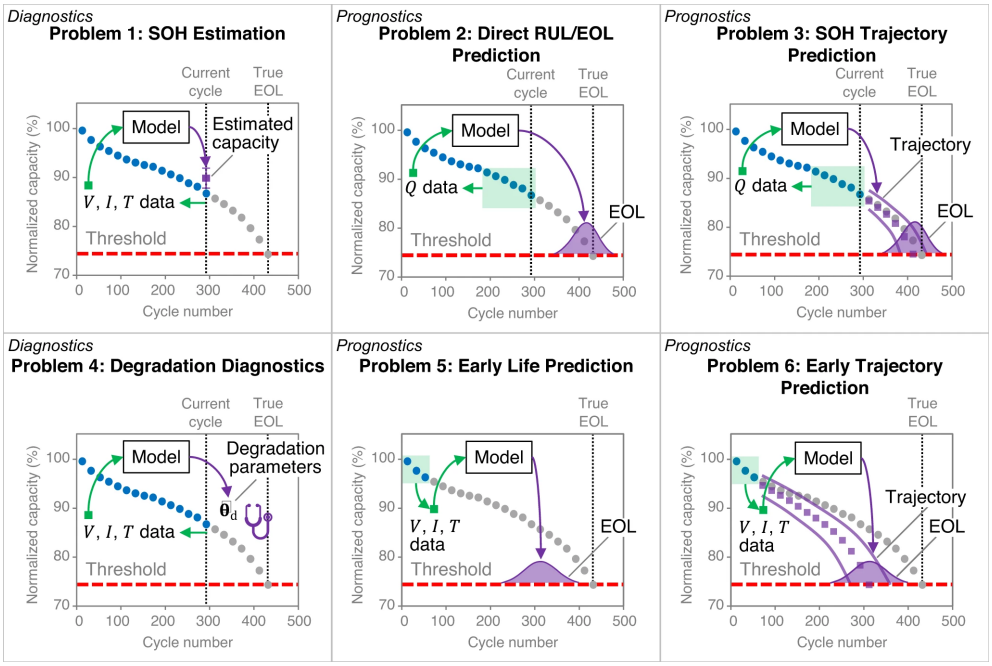

Figure 2.3: A series of plot showing the applications of data-driven methods employed for battery prognosis and diagnosis. Reproduced with permission from ref [42]. Copyright 2024 Nature.

in addition to cycling data to improve the predictive capabilities. On the other hand, Gaussian processes models can provide uncertainty interval, which helps in understanding the reliability and confidence of the predictions. [42,54].A significant body of research has also contributed to the development of hybrid models that combine the predictive capabilities of ML with the accuracy of PBM. [55–57] Consequently, a lot of emphasis is placed on holistic understanding the battery ageing and its contributing factors.

Deep learning and probabilistic models are often considered black-box techniques due to their limited transparency. [59] However, explainable or interpretable ML aims to provide insights into a model's decision-making process, thus enabling more reliable predictions. [60] In simple terms, explainable ML refers to describing the predictions in human terms, whereas interpretable ML involves understanding the inner mechanism of the model. [61] In the context of battery health prognosis and diagnosis, various methods have been explored to render ML models such as feature importance, correlations, Partial Dependence Plots (PDP) [62], Local Interpretable Model-Agnostic Explanations (LIME) [63] and SHapley Additive exPlanation (SHAP) [64]. Among these, SHAP is widely adopted because it can be applied to both local (individual) and global (overall) predictions. [60,65,66] Many studies utilize these methods to identify features from early cycling data that have the highest correlation with the target variable. [60] For instance,

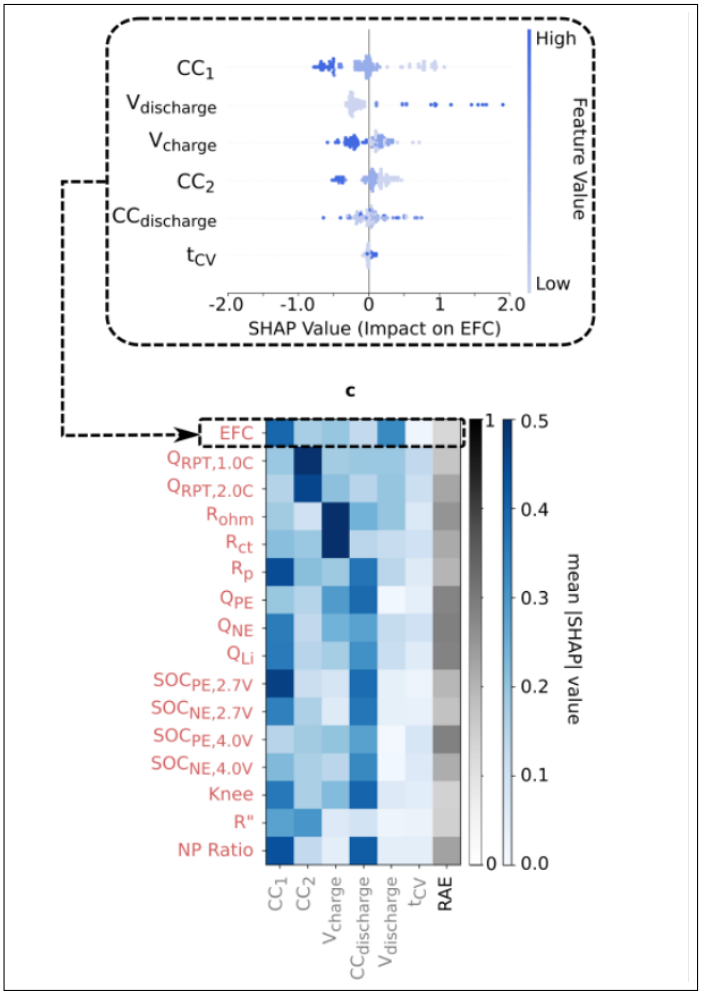

Figure 2.4: A schematic figure showing SHAP values between cycling parameters and equivalent full cycles (EFC) (top) and SOH metrics (bottom). Reproduced with permission from ref [58]. Copyright 2023 arXiv.

Lee *et al.* demonstrated that features derived from the 60th and 100th cycles show a high correlation to the SOH prediction at the 700th cycle. [64] This indicates that extracting features from early cycling data can significantly reduce computational efforts and enable robust predictions for later cycles. Additionally, SHAP has been employed to elucidate the convoluted degradation mechanisms occurring during cell aging. Vlijmen *et al.* showed the correlation between the cycling conditions and 16 SOH metrics. [58] Their work demonstrated that increasing cell resistance was attributed to the over-discharging of the positive electrode. However, it is still necessary to understand how different parameters effect cell aging over time to enable longer and safer battery life.

Although previous research has highlighted the individual effects of these parameters on cell degradation, their complex interactions during aging have not yet been thoroughly understood. In addressing this problem, a critical question arises, do bat-

teries undergo different degradation mechanism at different SOH levels? We find that utilizing explainable ML techniques can provide valuable insights into these intricate aging mechanisms. Recognizing that these parameters may exhibit correlations with each other during ageing, we also perform feature interaction measurement. This allows us find those features which have combined effect on cell degradation. Our work aims to offer a qualitative understanding of cell degradation, demonstrating a potential pathway to comprehend the underlying factors affecting battery health. By focusing on this subject, we hope to contribute to a deeper understanding of cell degradation and open doors for the development of longer-lasting batteries.

Chapter 3

Methods

3.1 Dataset

The dataset for this work is taken from the paper Burzyski *et al.* [67], who reported ageing tests on 28 $LiNi_{0.33}Mn_{0.33}Co_{0.33}$ - graphite cylindrical cells (18650 format). This particular dataset was selected for its extensive range of variables, such as ambient temperature, depth of discharge, discharge current, and average charging current, covering 26 diverse cycling conditions. Figure 3.1 provides a comparison between dataset from Poznan University (this work), MIT/Stanford/Toyota Research Institute (TRI) and Sandia National Laboratory (SNL). [68] In their work, the authors conducted capacity reference checks every two days to measure the state of health (SOH), where all the cells were tested until they reached 80% of nominal capacity (representing 0.80 SOH). Based on SOH values and the number of equivalent cycles (Neq), they introduced a novel cell aging parameter, *dSOH/dNeq*. This metric effectively captures cell ageing characteristics, as evidenced by its increasing value with decreasing SOH. This observation is consistent with the understanding that as the cell ages, the rate of degradation accelerates compared to a fresh cell. Furthermore, recognizing the dynamic nature of the solid-electrolyte interface (SEI) layer with cell ageing, the authors proposed the importance of using average charging current as a more accurate representation of charging conditions. A sample dataset for individual cell encompassing of different cycling parameters, SOH values ranging from 100% to 80% and *dSOH/dNeq* values is shown in table A.1.

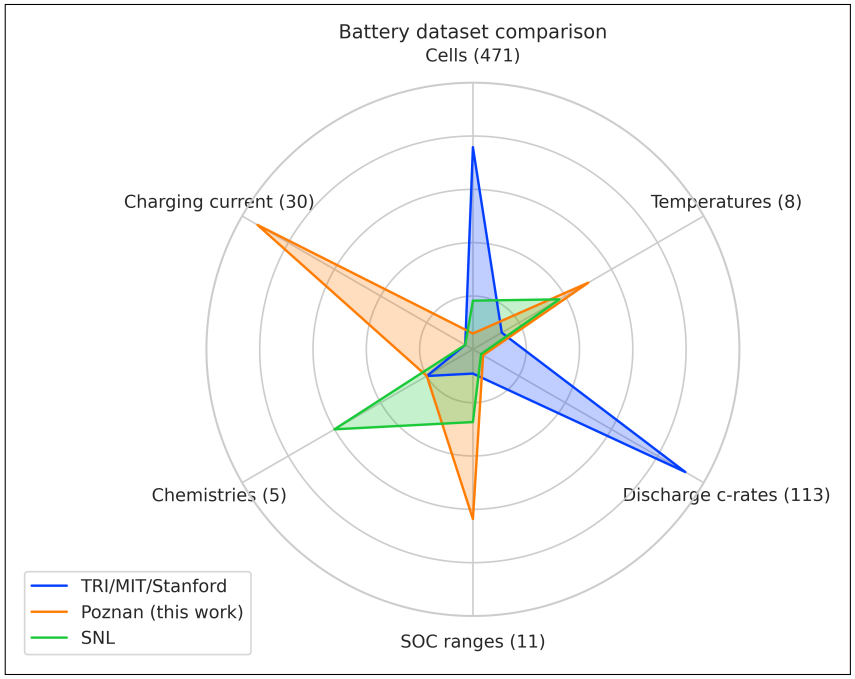

Figure 3.1: A spider plot comparing various open source datasets.

3.2 Data processing

To investigate the influence of parameters on degradation across different SOH levels, the dataset was partitioned into subsets based on identical SOH values for all cells. A representative subset for 0.95 SOH, encompassing data from all 28 cells, is presented in supplementary table A.2. Spearman's rank correlation coefficients and corresponding p-values were computed to assess the non-linear relationship between cycling conditions and cell degradation, as evidenced by previous studies. [69] To collectively capture these effects, all the cycling parameters from ageing tests were treated as input features, with *dSOH/dNeq* as the target output (figure 3.2a). Since the data downloaded from the study was already processed into a learning dataset, no further data processing was carried out apart from the partitioning explained above.

3.3 Machine learning modeling

Figure 3.2b outlines the machine learning modeling step subsequent to data segmentation. The authors originally employed Gaussian process regression (GPR) due to its effectiveness with small datasets, however, random forest regression was selected for this study owing to its superior interpretability and also the ability to capture non-linear

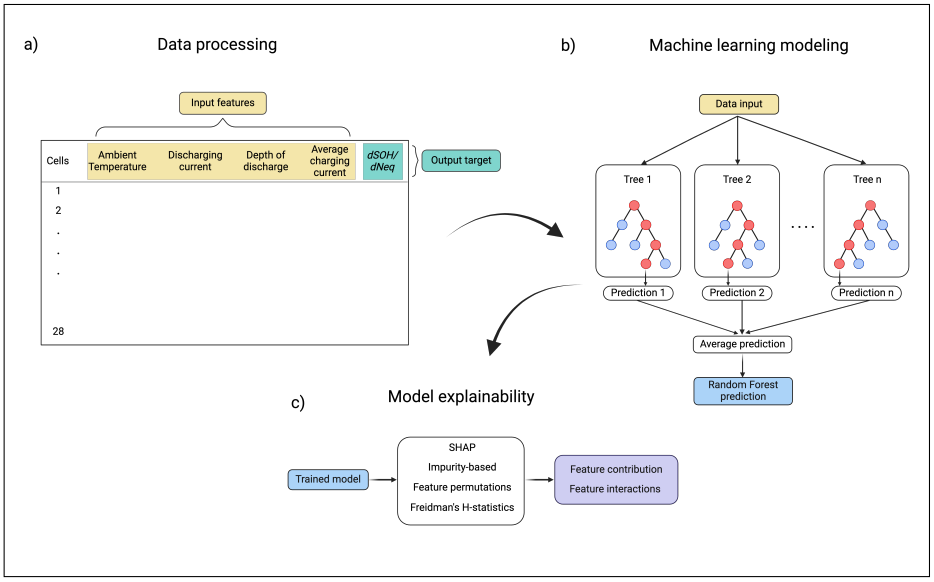

Figure 3.2: Schematic graphics showing the methodology of this work. a) Data processing the raw input file into learning dataset. b)Random forest model training. c) Model explainability in terms of feature importance and interactions.

relationships. For model training, all data points were considered to comprehensively examine the impact of diverse cycling parameters within the limited dataset. All the subsets were trained separately on random forest model to capture the unique degradation associated to that specific SOH. To mitigate the risk of over fitting associated with limited dataset, cross-validation scores were employed to assess model performance during hyperparameter optimization via grid search cross validation. However, the limited dataset and the actual values being close to zero can be misleading while measuring the model error A.1. Therefore, the model evaluation was conducted using several metrics, such as mean absolute error, explained variance score, R-squared, and root mean squared error, which are used to quantify prediction accuracy.

3.4 Model explainability

Feature importance is very common approach to understand the percentage contribution of features to the model predictions. Here we employ different methods to estimate the feature importance along with feature interactions, as cycling conditions can have some interactive effect on the degradation itself. Figure 3.2c illustrates variety of techniques such as SHAP, impurity-based indexing, permutation-based, and Friedman's H-statistic are employed to understand feature contribution and interaction.These techniques were applied to the trained model to measure the contribution and interac-

tions of cycling parameters on cell degradation across different SOH levels. The results from individual subsets were complied in a single stacked bar plot for straightforward comparison.

Chapter 4

Results and Discussion

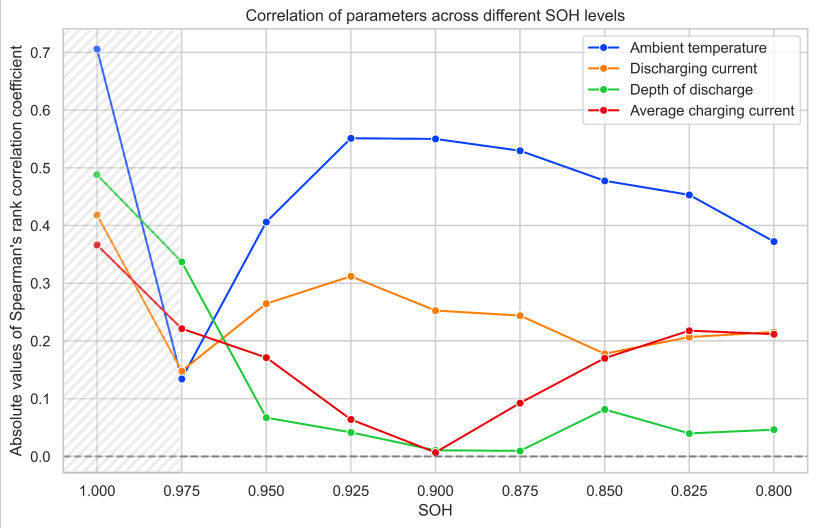

Figure 4.1: Spearman's rank correlation coefficients for all the cycling parameters from 1.00 to 0.80 SOH.

The initial data-analysis plots are presented to gain a better understanding of the data. Figure 4.1 shows the absolute Spearman's rank correlation coefficient (ρ_s) derived for all the subsets (figures A.3 to A.11). The ambient temperature has the the highest $|\rho_s|$, indicating the highest correlation with *dSOH/dNeq* and becomes more pronounced as cell ages. The general trend from correlation pattern is that, the discharge current has lower correlation relative to temperature, followed by charging current and depth of discharge.At 1.00 SOH, the *dSOH/dNeq* values are close to zero, as the cell undergoes negligible degradation. As a result, the impact of cycling conditions should

not be visible at this SOH, which may be misleading from the plot. Therefore, 1.00 SOH is shaded, and the same approach is followed in the remaining figures.

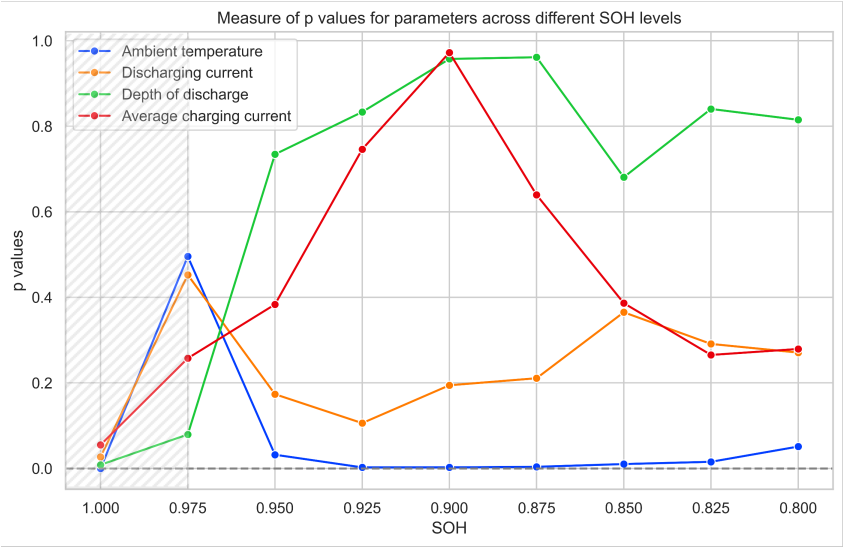

Figure 4.2: The calculated p-values for all the cycling parameters from 1.00 to 0.80 SOH.

Figure 4.2 presents the calculated p-values for each cycling parameters across different SOH's. Typically, p-values greater than 0.05 (threshold value) are considered statistically insignificant, implying that the parameters do not influence cell degradation. In their original study, Burzyski *et al.* demonstrated that all parameters had an impact cell degradation, as their calculated p-values were below 0.05. [67] However, based on our calculations, all the parameters exceeded the threshold values starting from 0.975 SOH except for ambient temperature. Here, again the p-values from 1.00 SOH are ignored as the degradation values were close zero. The reason for these contradictory results is that when the dataset is divided based on identical SOH, the resulting subsets have limited samples (28), which is nearly 10 times smaller than the original dataset (252). As highlighted by Gómez-de-Mariscal *et al.*, the p-values decreases with increase in data samples. [70] Therefore, all the parameters, even those with p-values greater than 0.05, were considered important due to their contextual and practical significance.

In Figure 4.3, the actual degradation values ($dSOH/dNeq$) are plotted against the predicted values from the random forest model, with colors indicating different subsets. Despite the small dataset of just 28 samples, the model demonstrates strong predictive capabilities without signs of overfitting. Additionally, tables A.3 and A.4 present the evaluation metrics for random forest regression and cross-validation scores showing

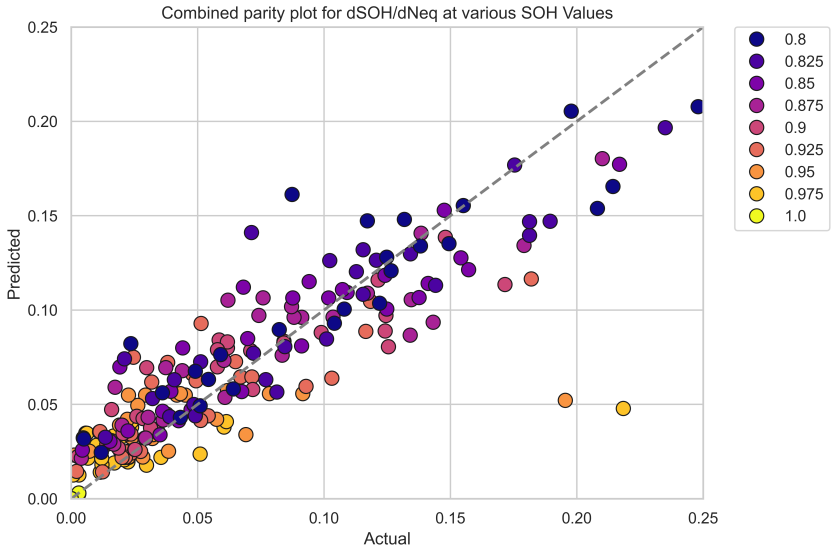

Figure 4.3: A combined parity plot for all the SOH subsets.

good fit of our model. The inconsistencies in evaluation score values are due to the target variable, *dSOH/dNeq*, being close to zero. To ensure a thorough evaluation of model fit in these scenarios, multiple metrics have been provided. Given the qualitative nature of this study, the focus has been primarily on understanding cell degradation rather than developing and applying new machine learning models for better predictions using limited dataset.

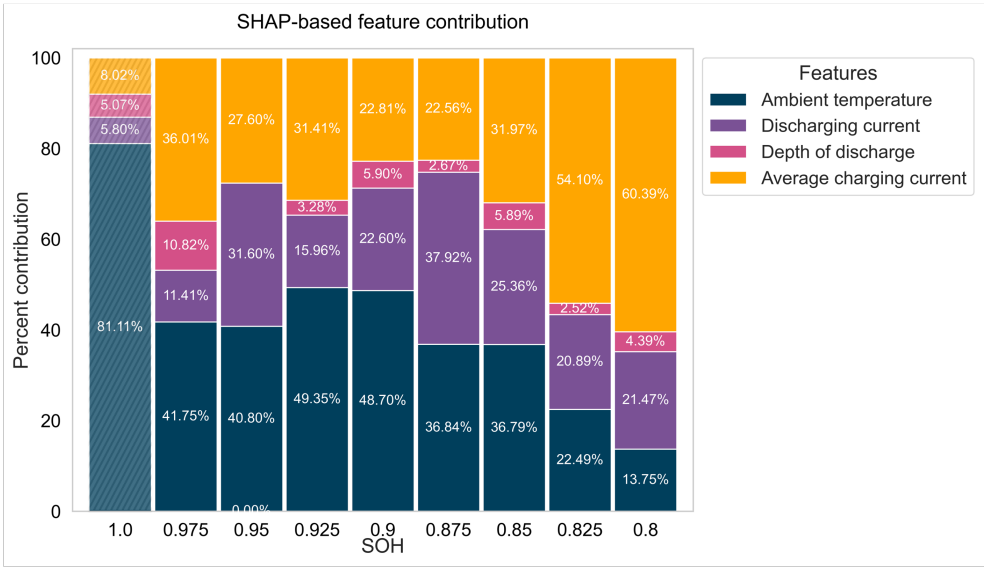

Figure 4.4: A stacked bar plot for SHAP based feature importance.

Figure 4.4, 4.5 and 4.6 show the feature importance plots describing the relative contribution of cycling parameters on cell degradation ($dSOH/dNeq$) as the cell ages from 1.00 to 0.80 SOH. SHAP, impurity-based index and permutation feature importance were employed to cross-validate the findings and corroborate our approach. SHAP calculates feature contribution based on Shapley values, which is the average marginal contribution of individual features across all the predictions. [71] Likewise, the impurity-based method estimates by averaging the total decrease in impurity measure caused by a specific feature across all trees in the random forest model. The permutation-based method relies on the model's prediction error when the features are permuted. Basically, features with more significant contributions to predictions result in high errors when shuffled.

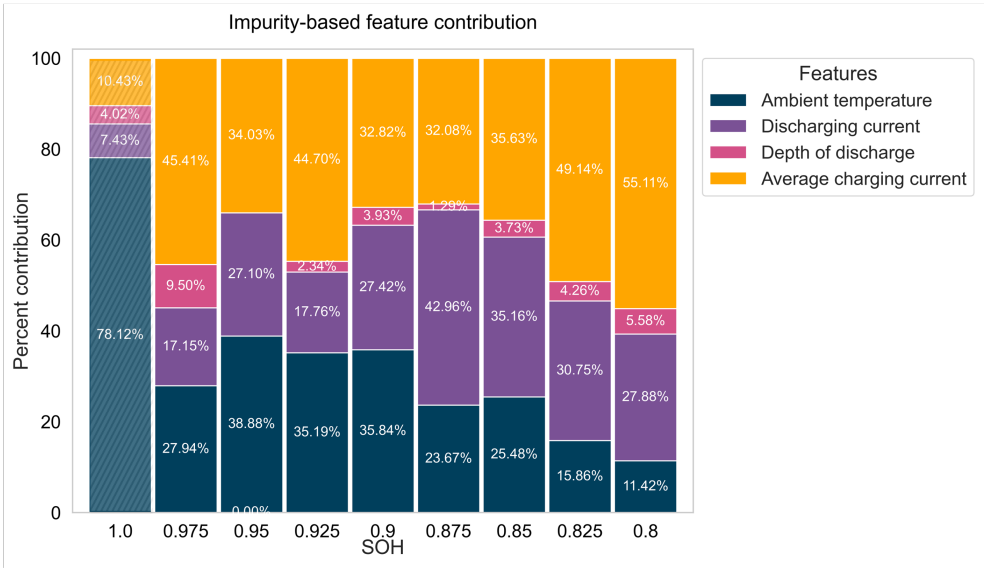

Figure 4.5: A stacked bar plot for impurity-based feature importance.

Figures 4.4, 4.6, and 4.5 show an evident decline in the contribution of temperature to degradation as the cell ages. Although the specific values vary depending on the feature contribution method, the overall trend remains consistent. The feature importance percentages decreases from 42% to 14% for SHAP, 28% to 11% impurity-based and 58% to 11% permutation-based. In contrast, the average charging current exhibits an increasing trend across all three approaches to cell aging. For SHAP, the value increases from 36% to 60%, 45% to 55% for impurity-based and 34% to 68% for permutation-based. The contribution of cycling parameters at 1.00 SOH is not considered is the analysis as degradation values at this SOH are almost zero. Based on the findings, we hypothesize that cycling parameters asymmetrically impact the cell degradation as it ages. Firstly, the sensitivity of temperature to cell degradation is extremely high from

0.975 to 0.90 SOH. Secondly, charging current has severe effects on degradation in the lower SOH region, from 0.875 to 0.80 SOH.

Figure 4.7 a, adopted from Preger *et al.*, shows a similar behavior for NMC cylindrical 18650 cells cycled at 25 and 35 °C. [13] The rate of capacity decay is reduced after reaching around 87% initial capacity (orange line), while the other cycling parameters are kept the same. The preferential susceptibility of fresh cells towards temperature is due to the large quantity of electrolyte available which is electrochemically reactive and conductive. As reported by Lai *et al*, the volume of electrolyte in cylindrical 18650 cell is directly related to its electrochemical performance. [72] Essentially, at higher temperatures the rapid electrolyte decomposition leads to an increase in the thickness of the solid electrolyte interphase (SEI) as shown in figure A.12 a and b. [9, 11] This growth in SEI layer results in increased internal resistance and a loss of lithium inventory. Similarly, at lower temperatures, lithium plating occurs due to decreased electrolyte viscosity and sluggish kinetics A.12 c and d. [11, 27, 73] As a result, the freshly deposited lithium, upon contact with the electrolyte, forms an SEI layer, eventually leading to increased cell resistance. [74] Hence, any change in temperature, either high or low will be the main driver for degradation.

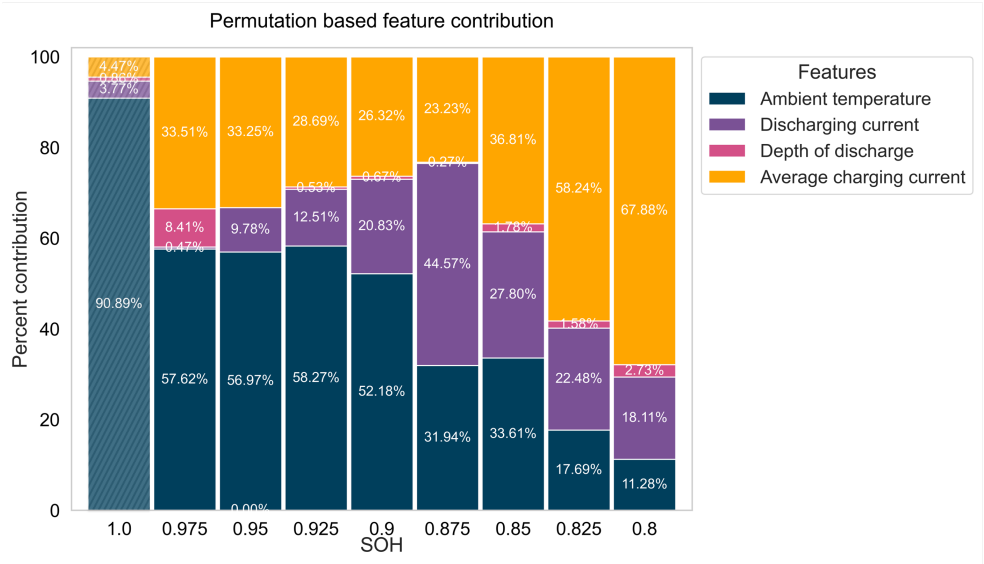

Figure 4.6: A stacked bar plot for permutation-based feature importance.

Beyond certain SOH (0.875 to 0.85), the charging current dominates the cell degradation that exceed the temperature contributions. As the cell ages, the conductive electrolyte is consumed in SEI formation [75], making the influence of temperature on cell degradation less significant. Moreover, Lall *et al.*, pointed out from their ageing

studies on NMC coin cells that charging current greatly contributes to cell degradation. [76] The high internal resistance in aged cells could cause more pronounced effects from charging currents, such as increased heat generation due to Joule hearing. [75, 77]. This temperature gradient within the cell causes uneven current density distribution, which leads to local degradation (figure A.13. [77] The stress induced by charging current can also result in loss of active material from mechanical degradation. [78] Figure 4.7, adopted from Guo *et al.*, shows the change in rate of decay of NMC 18650 cell after reaching 90% initial capacity (orange line). [79]

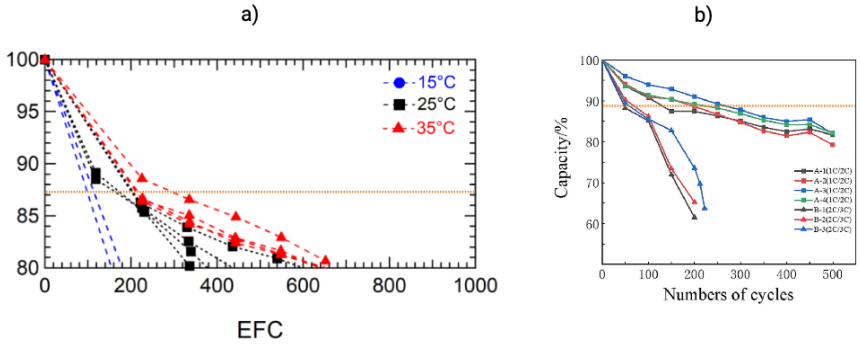

Figure 4.7: Influence of cycling parameters on capacity decay. a) The influence of temperature on cycle life of batteries and the orange line represents change in rate of degradation. Reproduced with permission from ref [9]. Copyright 2023 IOP Publishing. b) The influence of charging current on cycle life of batteries and the orange line represents change in rate of degradation. Reproduced with permission from ref [79]. Copyright 2019 Elsevier.

Usually, a large depth of discharge (DoD) can cause mechanical stress on battery materials due to expansion and contraction, resulting in LAM. [80] However, based on our feature importance analysis, we find that the effect of DoD is less than 10% in almost all cases. We believe that the effect of DoD on degradation becomes prominent only when the cell operates under baseline conditions, as shown in figure A.14. However, the effect of DoD is masked when operating at conditions higher than room temperature or with high charging currents. These factors can have a higher impact on degradation through mechanisms such as LLI or LAM, which is observed at high or low temperatures. In the context of charging current, the increased rate may lead to immediate stress on the electrode material, independent of DoD.

The cycling conditions can synergistically impact degradation. To fully understand the contributions of cycling parameters to degradation, we propose using H-statistics to measure feature interactions. These interactions between features can lead

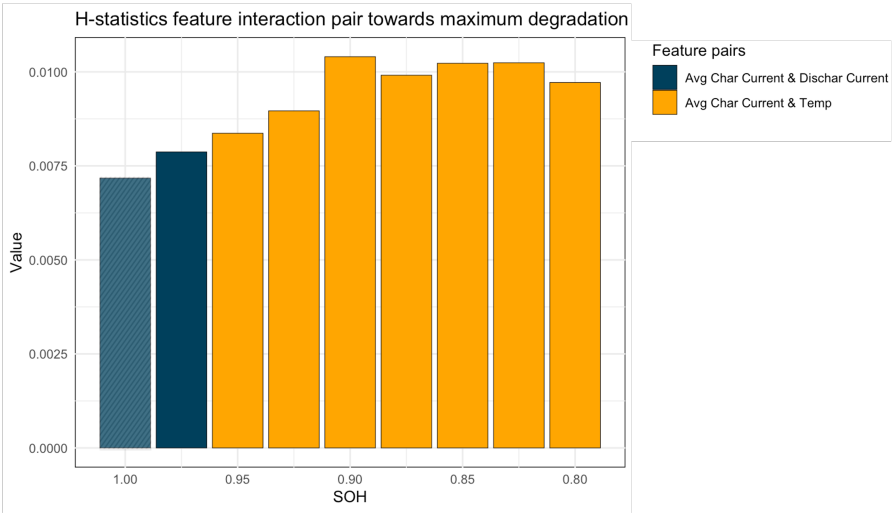

Figure 4.8: A bar plot for H-statistics based feature interactions.

to the combined degradation observed in the system. [81] The H-statistics values are dimensionless, meaning that higher values indicate stronger interactions between two features. Figure 4.8 presents the features with the highest interaction values. Notably, for almost every SOH levels, average charging current and temperature exhibit significant interactions. This aligns with the earlier observation that either temperature or charging current significantly contributes to degradation. Accordingly, we should observe the degradation effect arising either in combination with temperature, charging current, or both. However, at a 0.975 SOH, we observe a higher interaction between charging current and discharge current, which may indicate an error or discrepancy. To validate the accuracy of the H-statistics results, feature importance derived from the same method is presented in figure A.15, showing consistency with the previous trends.

Chapter 5

Conclusion

In this study, we reported the use of explainable machine learning to understand the impact of cycling conditions at different stages of SOH. We propose that the degradation is driven by different cycling parameters at different stages of SOH as shown in figure 5.1. All feature importance methods suggested that temperature is a dominant factor causing degradation during the early stages of cycle life, from 1.00 to 0.900 SOH. We propose that the large quantity of electrolyte available during these early stages is highly reactive and undergoes side reactions, leading to LLI. As the battery ages, this electrolyte is consumed to form an interficial layer, which increases resistance. Therefore, from 0.875 to 0.800 SOH, degradation is no longer dominated by temperature, as there is insufficient electrolyte to undergo decomposition reactions. At this stage, degradation becomes more sensitive to charging current because the existing non-uniform layer induces an uneven distribution of current. This results in localized heating, such as Joule heating that causes cell degradation. We also utilized feature interaction measures to quantify the interactive effects of various parameters on degradation. The results suggest that the combination of average charging current and temperature significantly contributes to degradation, which corroborates our feature importance analysis. Through this study, we provide a comprehensive understanding of the contribution and interaction of cycling parameters leading to degradation across different SOH ranges. By identifying temperature and charging current as key factors influencing degradation, and quantifying their interactions, we pave the way for more targeted strategies to extend battery life and safety.

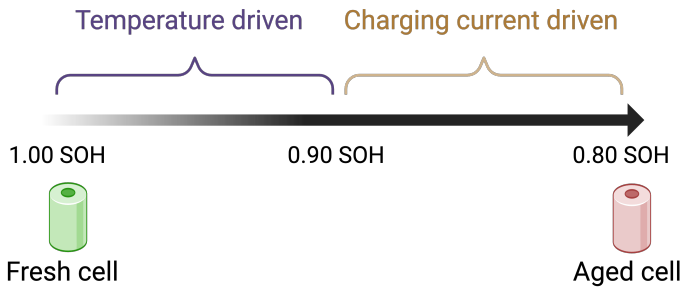

Figure 5.1: Schematic illustration showing the summary of our findings

Currently, our findings are limited to a specific chemistry (NMC) and cell format (18650). Our findings underscore the importance of employing small dataset with advanced data-driven methods to uncover complex degradation in batteries. With more experimental data from cycling studies under diverse operating conditions, we can develop robust data-driven methods that provide insights into degradation mechanisms and offer foresight to optimize battery aging.

References

[1] James T. Frith, Matthew J. Lacey, and Ulderico Ulissi. A non-academic perspective on the future of lithium-based batteries. *Nature Communications*, 14(1), January 2023.

[2] Trends in electric vehicle batteries – Global EV Outlook 2024 – Analysis - IEA — iea.org. https://www.iea.org/reports/global-ev-outlook-2024/trends-in-electric-vehicle-batteries. [Accessed 04-08-2024].

[3] Yangtao Liu, Ruihan Zhang, Jun Wang, and Yan Wang. Current and future lithium-ion battery manufacturing. *iScience*, 24(4):102332, April 2021.

[4] Jiangong Zhu, Wentao Xu, Michael Knapp, Mariyam Susana Dewi Darma, Liuda Mereacre, Peiji Su, Weibo Hua, Xinyang Liu-Théato, Haifeng Dai, Xuezhe Wei, and Helmut Ehrenberg. A method to prolong lithium-ion battery life during the full life cycle. *Cell Reports Physical Science*, 4(7):101464, July 2023.

[5] M. Rosa Palacín. Understanding ageing in li-ion batteries: a chemical issue. *Chemical Society Reviews*, 47(13):4924–4933, 2018.

[6] Christoph R. Birkl, Matthew R. Roberts, Euan McTurk, Peter G. Bruce, and David A. Howey. Degradation diagnostics for lithium ion cells. *Journal of Power Sources*, 341:373–386, February 2017.

[7] J. Vetter, P. Novák, M.R. Wagner, C. Veit, K.-C. Möller, J.O. Besenhard, M. Winter, M. Wohlfahrt-Mehrens, C. Vogler, and A. Hammouche. Ageing mechanisms in lithium-ion batteries. *Journal of Power Sources*, 147(1–2):269–281, September 2005.

[8] Amartya Mukhopadhyay and Brian W. Sheldon. Deformation and stress in electrode materials for li-ion batteries. *Progress in Materials Science*, 63:58–116, June 2014.

[9] Reed Wittman, Matthieu Dubarry, Sergei Ivanov, Benjamin W. Juba, Jessica Romàn-Kustas, Armando Fresquez, Jill Langendorf, Richard Grant, Gretchen Taggart, Babu Chalamala, and Yuliya Preger. Characterization of cycle-aged commercial

nmc and nca lithium-ion cells: I. temperature-dependent degradation. *Journal of The Electrochemical Society*, 170(12):120538, December 2023.

[10] M. Broussely, Ph. Biensan, F. Bonhomme, Ph. Blanchard, S. Herreyre, K. Nechev, and R.J. Staniewicz. Main aging mechanisms in li ion batteries. *Journal of Power Sources*, 146(1–2):90–96, August 2005.

[11] Thomas Waldmann, Marcel Wilka, Michael Kasper, Meike Fleischhammer, and Margret Wohlfahrt-Mehrens. Temperature dependent ageing mechanisms in lithium-ion batteries – a post-mortem study. *Journal of Power Sources*, 262:129–135, September 2014.

[12] Madeleine Ecker, Nerea Nieto, Stefan Käbitz, Johannes Schmalstieg, Holger Blanke, Alexander Warnecke, and Dirk Uwe Sauer. Calendar and cycle life study of li(nimnco)o2-based 18650 lithium-ion batteries. *Journal of Power Sources*, 248:839–851, February 2014.

[13] Yuliya Preger, Heather M. Barkholtz, Armando Fresquez, Daniel L. Campbell, Benjamin W. Juba, Jessica Romàn-Kustas, Summer R. Ferreira, and Babu Chalamala. Degradation of commercial lithium-ion cells as a function of chemistry and cycling conditions. *Journal of The Electrochemical Society*, 167(12):120532, January 2020.

[14] J.G. Qu, Z.Y. Jiang, and J.F. Zhang. Investigation on lithium-ion battery degradation induced by combined effect of current rate and operating temperature during fast charging. *Journal of Energy Storage*, 52:104811, August 2022.

[15] A. Pfrang, A. Kersys, A. Kriston, D.U. Sauer, C. Rahe, S. Käbitz, and E. Figgemeier. Long-term cycling induced jelly roll deformation in commercial 18650 cells. *Journal of Power Sources*, 392:168–175, July 2018.

[16] Seung-Taek Myung, Yashiro Hitoshi, and Yang-Kook Sun. Electrochemical behavior and passivation of current collectors in lithium-ion batteries. *Journal of Materials Chemistry*, 21(27):9891, 2011.

[17] Christopher L. Campion, Wentao Li, and Brett L. Lucht. Thermal decomposition of lipf[sub 6]-based electrolytes for lithium-ion batteries. *Journal of The Electrochemical Society*, 152(12):A2327, 2005.

[18] Yiqing Liao, Huiyan Zhang, Yufan Peng, Yonggang Hu, Jinding Liang, Zhengliang Gong, Yimin Wei, and Yong Yang. Electrolyte degradation during aging process of lithium-ion batteries: Mechanisms, characterization, and quantitative analysis. *Advanced Energy Materials*, 14(18), February 2024.

[19] Toby Bond, Roby Gauthier, A. Eldesoky, Jessie Harlow, and J. R. Dahn. In situ imaging of electrode thickness growth and electrolyte depletion in single-crystal vs polycrystalline linixmnycozo2/graphite pouch cells using multi-scale computed tomography. *Journal of The Electrochemical Society*, 169(2):020501, February 2022.

[20] Richard Stockhausen, Lydia Gehrlein, Marcus Müller, Thomas Bergfeldt, Andreas Hofmann, Freya Janina Müller, Julia Maibach, Helmut Ehrenberg, and Anna Smith. Investigating the dominant decomposition mechanisms in lithium-ion battery cells responsible for capacity loss in different stages of electrochemical aging. *Journal of Power Sources*, 543:231842, September 2022.

[21] Huw C. W. Parks, Adam M. Boyce, Aaron Wade, Thomas M. M. Heenan, Chun Tan, Emilio Martínez-Pañeda, Paul R. Shearing, Dan J. L. Brett, and Rhodri Jervis. Direct observations of electrochemically induced intergranular cracking in polycrystalline nmc811 particles. *Journal of Materials Chemistry A*, 11(39):21322–21332, 2023.

[22] Amartya Mukhopadhyay, Anton Tokranov, Xingcheng Xiao, and Brian W. Sheldon. Stress development due to surface processes in graphite electrodes for li-ion batteries: A first report. *Electrochimica Acta*, 66:28–37, April 2012.

[23] Aleksandr O. Kondrakov, Alexander Schmidt, Jin Xu, Holger Geßwein, Reiner Mönig, Pascal Hartmann, Heino Sommer, Torsten Brezesinski, and Jürgen Janek. Anisotropic lattice strain and mechanical degradation of high- and low-nickel ncm cathode materials for li-ion batteries. *The Journal of Physical Chemistry C*, 121(6):3286–3294, February 2017.

[24] Anu Adamson, Kenneth Tuul, Tom Bötticher, Saad Azam, Matthew D. L. Garayt, and Michael Metzger. Improving lithium-ion cells by replacing polyethylene terephthalate jellyroll tape. *Nature Materials*, 22(11):1380–1386, September 2023.

[25] Liya Guo, Daisy B Thornton, Mohamed A Koronfel, Ifan E L Stephens, and Mary P Ryan. Degradation in lithium ion battery current collectors. *Journal of Physics: Energy*, 3(3):032015, July 2021.

[26] Feng Leng, Cher Ming Tan, and Michael Pecht. Effect of temperature on the aging rate of li ion battery operating above room temperature. *Scientific Reports*, 5(1), August 2015.

[27] E. Teliz, C. López-Vázquez, and V. Díaz. Degradation study for 18650 nmc batteries at low temperature. *Electrochimica Acta*, 475:143540, January 2024.

[28] Alexis Laforgue, Xiao-Zi Yuan, Alison Platt, Shawn Brueckner, Florence Perrin-Sarazin, Mathieu Toupin, Jean-Yves Huot, and Asmae Mokrini. Effects of fast charging at low temperature on a high energy li-ion battery. *Journal of The Electrochemical Society*, 167(14):140521, November 2020.

[29] Man-Fai Ng, Jin Zhao, Qingyu Yan, Gareth J. Conduit, and Zhi Wei Seh. Predicting the state of charge and health of batteries using data-driven machine learning. *Nature Machine Intelligence*, 2(3):161–170, March 2020.

[30] Martin Petit, Eric Prada, and Valérie Sauvant-Moynot. Development of an empirical aging model for li-ion batteries and application to assess the impact of vehicle-to-grid strategies on battery lifetime. *Applied Energy*, 172:398–407, June 2016.

[31] M. Safari, M. Morcrette, A. Teyssot, and C. Delacourt. Multimodal physics-based aging model for life prediction of li-ion batteries. *Journal of The Electrochemical Society*, 156(3):A145, 2009.

[32] Jorn M. Reniers, Grietus Mulder, and David A. Howey. Review and performance comparison of mechanical-chemical degradation models for lithium-ion batteries. *Journal of The Electrochemical Society*, 166(14):A3189–A3200, 2019.

[33] Simon E. J. O'Kane, Weilong Ai, Ganesh Madabattula, Diego Alonso-Alvarez, Robert Timms, Valentin Sulzer, Jacqueline Sophie Edge, Billy Wu, Gregory J. Offer, and Monica Marinescu. Lithium-ion battery degradation: how to model it. *Physical Chemistry Chemical Physics*, 24(13):7909–7922, 2022.

[34] Joris de Hoog, Jean-Marc Timmermans, Daniel Ioan-Stroe, Maciej Swierczynski, Joris Jaguemont, Shovon Goutam, Noshin Omar, Joeri Van Mierlo, and Peter Van Den Bossche. Combined cycling and calendar capacity fade modeling of a nickel-manganese-cobalt oxide cell with real-life profile validation. *Applied Energy*, 200:47–61, August 2017.

[35] Rui Xiong, Jiayi Cao, Quanqing Yu, Hongwen He, and Fengchun Sun. Critical review on the battery state of charge estimation methods for electric vehicles. *IEEE Access*, 6:1832–1843, 2018.

[36] Penelope K. Jones, Ulrich Stimming, and Alpha A. Lee. Impedance-based forecasting of lithium-ion battery performance amid uneven usage. *Nature Communications*, 13(1), August 2022.

[37] Thomas F. Fuller, Marc Doyle, and John Newman. Simulation and optimization of the dual lithium ion insertion cell. *Journal of The Electrochemical Society*, 141(1):1–10, January 1994.

[38] Matthew B. Pinson and Martin Z. Bazant. Theory of sei formation in rechargeable batteries: Capacity fade, accelerated aging and lifetime prediction. *Journal of The Electrochemical Society*, 160(2):A243–A250, December 2012.

[39] Xiao-Guang Yang, Yongjun Leng, Guangsheng Zhang, Shanhai Ge, and Chao-Yang Wang. Modeling of lithium plating induced aging of lithium-ion batteries: Transition from linear to nonlinear aging. *Journal of Power Sources*, 360:28–40, August 2017.

[40] Venkatasailanathan Ramadesigan, Kejia Chen, Nancy A. Burns, Vijayasekaran Boovaragavan, Richard D. Braatz, and Venkat R. Subramanian. Parameter estimation and capacity fade analysis of lithium-ion batteries using reformulated models. *Journal of The Electrochemical Society*, 158(9):A1048, 2011.

[41] Arthur von Wald Cresce, Oleg Borodin, and Kang Xu. Correlating li+ solvation sheath structure with interphasial chemistry on graphite. *The Journal of Physical Chemistry C*, 116(50):26111–26117, December 2012.

[42] Adam Thelen, Xun Huan, Noah Paulson, Simona Onori, Zhen Hu, and Chao Hu. Probabilistic machine learning for battery health diagnostics and prognostics—review and perspectives. *npj Materials Sustainability*, 2(1), June 2024.

[43] Xiaosong Hu, Le Xu, Xianke Lin, and Michael Pecht. Battery lifetime prognostics. *Joule*, 4(2):310–346, February 2020.

[44] Huixin Tian, Pengliang Qin, Kun Li, and Zhen Zhao. A review of the state of health for lithium-ion batteries: Research status and suggestions. *Journal of Cleaner Production*, 261:120813, July 2020.

[45] Yi Li, Kailong Liu, Aoife M. Foley, Alana Zülke, Maitane Berecibar, Elise Nanini-Maury, Joeri Van Mierlo, and Harry E. Hoster. Data-driven health estimation and lifetime prediction of lithium-ion batteries: A review. *Renewable and Sustainable Energy Reviews*, 113:109254, October 2019.

[46] Peter M. Attia, Alexander Bills, Ferran Brosa Planella, Philipp Dechent, Gonçalo dos Reis, Matthieu Dubarry, Paul Gasper, Richard Gilchrist, Samuel Greenbank, David Howey, Ouyang Liu, Edwin Khoo, Yuliya Preger, Abhishek Soni, Shashank Sripad, Anna G. Stefanopoulou, and Valentin Sulzer. Review—"knees" in lithium-ion battery aging trajectories. *Journal of The Electrochemical Society*, 169(6):060517, June 2022.

[47] Kristen A. Severson, Peter M. Attia, Norman Jin, Nicholas Perkins, Benben Jiang, Zi Yang, Michael H. Chen, Muratahan Aykol, Patrick K. Herring, Dimitrios

Fraggedakis, Martin Z. Bazant, Stephen J. Harris, William C. Chueh, and Richard D. Braatz. Data-driven prediction of battery cycle life before capacity degradation. *Nature Energy*, 4(5):383–391, March 2019.

[48] Yunwei Zhang, Qiaochu Tang, Yao Zhang, Jiabin Wang, Ulrich Stimming, and Alpha A. Lee. Identifying degradation patterns of lithium ion batteries from impedance spectroscopy using machine learning. *Nature Communications*, 11(1), April 2020.

[49] Paula Fermín-Cueto, Euan McTurk, Michael Allerhand, Encarni Medina-Lopez, Miguel F. Anjos, Joel Sylvester, and Gonçalo dos Reis. Identification and machine learning prediction of knee-point and knee-onset in capacity degradation curves of lithium-ion cells. *Energy and AI*, 1:100006, August 2020.

[50] Jiahuan Lu, Rui Xiong, Jinpeng Tian, Chenxu Wang, and Fengchun Sun. Deep learning to estimate lithium-ion battery state of health without additional degradation experiments. *Nature Communications*, 14(1), May 2023.

[51] Mehrad Ansari, Steven B. Torrisi, Amalie Trewartha, and Shijing Sun. History-agnostic battery degradation inference. *Journal of Energy Storage*, 81:110279, March 2024.

[52] Greg Davies, Kevin W. Knehr, Barry Van Tassell, Thomas Hodson, Shaurjo Biswas, Andrew G. Hsieh, and Daniel A. Steingart. State of charge and state of health estimation using electrochemical acoustic time of flight analysis. *Journal of The Electrochemical Society*, 164(12):A2746–A2755, 2017.

[53] Kevin W. Knehr, Thomas Hodson, Clement Bommier, Greg Davies, Andrew Kim, and Daniel A. Steingart. Understanding full-cell evolution and non-chemical electrode crosstalk of li-ion batteries. *Joule*, 2(6):1146–1159, June 2018.

[54] Robert R. Richardson, Michael A. Osborne, and David A. Howey. Gaussian process regression for forecasting battery state of health. *Journal of Power Sources*, 357:209–219, July 2017.

[55] Muratahan Aykol, Chirranjeevi Balaji Gopal, Abraham Anapolsky, Patrick K. Herring, Bruis van Vlijmen, Marc D. Berliner, Martin Z. Bazant, Richard D. Braatz, William C. Chueh, and Brian D. Storey. Perspective—combining physics and machine learning to predict battery lifetime. *Journal of The Electrochemical Society*, 168(3):030525, March 2021.

[56] Jinpeng Tian, Rui Xiong, Jiahuan Lu, Cheng Chen, and Weixiang Shen. Battery state-of-charge estimation amid dynamic usage with physics-informed deep learning. *Energy Storage Materials*, 50:718–729, September 2022.

[57] Linxia Liao and Felix Köttig. Review of hybrid prognostics approaches for remaining useful life prediction of engineered systems, and an application to battery life prediction. *IEEE Transactions on Reliability*, 63(1):191–207, 2014.

[58] Bruis van Vlijmen, Vivek Lam, Patrick A. Asinger, Xiao Cui, Devi Ganapathi, Shijing Sun, Patrick K. Herring, Chirranjeevi Balaji Gopal, Natalie Geise, Haitao D. Deng, Henry L. Thaman, Stephen Dongmin Kang, Amalie Trewartha, Abraham Anapolsky, Brian D. Storey, William E. Gent, Richard D. Braatz, and William C. Chueh. Interpretable data-driven modeling reveals complexity of battery aging. *arXiv*, May 2023.

[59] Chang Wang, Ying Chen, Weiling Luan, Songyang Li, Yiming Yao, and Haofeng Chen. Interpretable deep learning for accelerated fading recognition of lithium-ion batteries. *eTransportation*, 18:100281, October 2023.

[60] Mona Faraji Niri, Koorosh Aslansefat, Sajedeh Haghi, Mojgan Hashemian, Rüdiger Daub, and James Marco. A review of the applications of explainable machine learning for lithium–ion batteries: From production to state and performance estimation. *Energies*, 16(17):6360, September 2023.

[61] Interpretability versus explainability - Model Explainability with AWS Artificial Intelligence and Machine Learning Solutions — docs.aws.amazon.com. https://docs.aws.amazon.com/whitepapers/latest/model-explainability-aws-ai-ml/interpretability-versus-explainability.html. [Accessed 10-08-2024].

[62] Huang Zhang, Yang Su, Faisal Altaf, Torsten Wik, and Sébastien Gros. Interpretable battery cycle life range prediction using early cell degradation data. *IEEE Transactions on Transportation Electrification*, 9(2):2669–2682, 2023.

[63] Shiva Teja Rapolu, Umesh Chandra Kadali, Jashwanth Vemula, Aparna Sinha, and Debanjan Das. Interpretable deep learning approach for long horizon health prognosis of a li-ion battery. In *2023 IEEE 20th India Council International Conference (INDICON)*, pages 334–339, 2023.

[64] Gyumin Lee, Juram Kim, and Changyong Lee. State-of-health estimation of li-ion batteries in the early phases of qualification tests: An interpretable machine learning approach. *Expert Systems with Applications*, 197:116817, July 2022.

[65] Fu Jiang, Youzhi He, Dianzhu Gao, Yun Zhou, Weirong Liu, Lisen Yan, and Jun Peng. An accurate and interpretable lifetime prediction method for batteries using extreme gradient boosting tree and treeexplainer. In *2021 IEEE 23rd Int Conf on*

High Performance Computing & Communications; 7th Int Conf on Data Science & Systems; 19th Int Conf on Smart City; 7th Int Conf on Dependability in Sensor, Cloud & Big Data Systems & Application (HPCC/DSS/SmartCity/DependSys), pages 1042–1048, 2021.

[66] Guanzheng Li, Bin Li, Chao Li, and Shuai Wang. State-of-health rapid estimation for lithium-ion battery based on an interpretable stacking ensemble model with short-term voltage profiles. *Energy*, 263:126064, January 2023.

[67] Damian Burzyński and Leszek Kasprzyk. A novel method for the modeling of the state of health of lithium-ion cells using machine learning for practical applications. *Knowledge-Based Systems*, 219:106900, May 2021.

[68] Gonçalo dos Reis, Calum Strange, Mohit Yadav, and Shawn Li. Lithium-ion battery data and where to find it. *Energy and AI*, 5:100081, September 2021.

[69] Simon F. Schuster, Tobias Bach, Elena Fleder, Jana Müller, Martin Brand, Gerhard Sextl, and Andreas Jossen. Nonlinear aging characteristics of lithium-ion cells under different operational conditions. *Journal of Energy Storage*, 1:44–53, June 2015.

[70] Estibaliz Gómez-de Mariscal, Vanesa Guerrero, Alexandra Sneider, Hasini Jayatilaka, Jude M. Phillip, Denis Wirtz, and Arrate Muñoz-Barrutia. Use of the p-values as a size-dependent function to address practical differences when analyzing large datasets. *Scientific Reports*, 11(1), October 2021.

[71] Scott M. Lundberg, Gabriel Erion, Hugh Chen, Alex DeGrave, Jordan M. Prutkin, Bala Nair, Ronit Katz, Jonathan Himmelfarb, Nisha Bansal, and Su-In Lee. From local explanations to global understanding with explainable ai for trees. *Nature Machine Intelligence*, 2(1):56–67, January 2020.

[72] Xin Lai, Yunfei Li, Ruqing Fang, Peng Dong, Yuejiu Zheng, and Zhe Li. Experimental investigation of the influence of electrolyte loss and replenishment on the critical performances of cylindrical lithium-ion cells. *J. Energy Storage*, 52(104951):104951, August 2022.

[73] Guangxu Zhang, Xuezhe Wei, Guangshuai Han, Haifeng Dai, Jiangong Zhu, Xueyuan Wang, Xuan Tang, and Jiping Ye. Lithium plating on the anode for lithium-ion batteries during long-term low temperature cycling. *J. Power Sources*, 484(229312):229312, February 2021.

[74] Arpit Maheshwari, Michael Heck, and Massimo Santarelli. Cycle aging studies of lithium nickel manganese cobalt oxide-based batteries using electrochemical impedance spectroscopy. *Electrochimica Acta*, 273:335–348, May 2018.

[75] Joris De Hoog, Joris Jaguemont, Mohamed Abdel-Monem, Peter Van Den Bossche, Joeri Van Mierlo, and Noshin Omar. Combining an electrothermal and impedance aging model to investigate thermal degradation caused by fast charging. *Energies*, 11(4):804, March 2018.

[76] Pradeep Lall, Ved Soni, Guneet Sethi, and Kok Yiang. SOH modelling of li-ion coin cells subjected to varying c-rates, depths of charge, operating temperatures and custom charge profiles. In *2021 20th IEEE Intersociety Conference on Thermal and Thermomechanical Phenomena in Electronic Systems (iTherm)*. IEEE, June 2021.

[77] Anna Tomaszewska, Zhengyu Chu, Xuning Feng, Simon O'Kane, Xinhua Liu, Jingyi Chen, Chenzhen Ji, Elizabeth Endler, Ruihe Li, Lishuo Liu, Yalun Li, Siqi Zheng, Sebastian Vetterlein, Ming Gao, Jiuyu Du, Michael Parkes, Minggao Ouyang, Monica Marinescu, Gregory Offer, and Billy Wu. Lithium-ion battery fast charging: A review. *eTransportation*, 1(100011):100011, August 2019.

[78] Wenlong Xie, Rong He, Xinlei Gao, Xinghu Li, Huizhi Wang, Xinhua Liu, Xiaoyu Yan, and Shichun Yang. Degradation identification of LiNi0.8Co0.1Mn0.1O2/graphite lithium-ion batteries under fast charging conditions. *Electrochim. Acta*, 392(138979):138979, October 2021.

[79] Yibo Guo, Jinle Cai, Yunlong Liao, Jiahua Hu, and Xiaomeng Zhou. Insight into fast charging/discharging aging mechanism and degradation-safety analytics of 18650 lithium-ion batteries. *J. Energy Storage*, 72(108331):108331, November 2023.

[80] Roby Gauthier, Aidan Luscombe, Toby Bond, Michael Bauer, Michel Johnson, Jessie Harlow, Alex Louli, and Jeff R Dahn. How do depth of discharge, c-rate and calendar age affect capacity retention, impedance growth, the electrodes, and the electrolyte in li-ion cells? *Journal of The Electrochemical Society*, January 2022.

[81] Jerome H. Friedman and Bogdan E. Popescu. Predictive learning via rule ensembles. *The Annals of Applied Statistics*, 2(3), September 2008.

Appendix A

Supplementry

Table A.1: A sample dataset for cell 1

cell_name	Ambient temperature	Discharging current	Depth of discharge	Average charging current	State of Health	$dSOH/dNeq$
1	10	-2.6	73	2.6	1	0.003
	10	-2.6	73	2.53	0.975	0.022
	10	-2.6	73	2.44	0.95	0.0418
	10	-2.6	73	2.41	0.925	0.067
	10	-2.6	73	2.33	0.9	0.0841651
	10	-2.6	73	2.33	0.875	0.10356371
	10	-2.6	73	2.28	0.85	0.10915
	10	-2.6	73	2.1915	0.825	0.11548
	10	-2.6	73	2.15	0.8	0.12653664

Table A.2: A sample subset for all the 28 cells at 0.95 SOH

cell_name	Ambient temperature	Discharging current	Depth of discharge	Average charging current	$dSOH/dNeq$
1	10	-2.6	73	2.44	0.0418
2	10	-2.6	50	2.22	0.02942
3	10	-2.6	27	1.63	0.04513
4	10	-2.6	100	2.52	0.0618
5	10	-7.8	100	2.82	0.19546
6	10	-5.2	60	1.75	0.02634
7	10	-2.6	67	1.59	0.02265
8	15	-2.6	100	1.93	0.02222
9	15	-5.2	100	2.38	0.03208
10	15	-7.8	100	3.02	0.01965
11	15	-5.2	50	2.21	0.03241
12	15	-2.6	50	2.02	0.05751
13	15	-5.2	100	1.86	0.0691
14	25	-10.5	100	2.12	0.0385
15	25	-7.8	100	3.07	0.0239
16	25	-5.2	100	2.73	0.02271
17	25	-2.6	100	1.95	0.0112
18	25	-7.8	100	1.84	0.01947
19	25	-5.2	100	2.03	0.02269
20	25	-2.6	100	3.10	0.07841
21	25	-5.2	50	2.18	0.00715
22	25	-5.2	16	2.35	0.00122
23	40	-7.8	100	3.08	0.0191
24	40	-5.2	100	2.88	0.01584
25	40	-2.6	100	2.40	0.02153
26	40	-2.6	100	3.59	0.04318
27	25	-2.6	100	3.41	0.0916
28	40	-3.9	100	2.703	0.02831

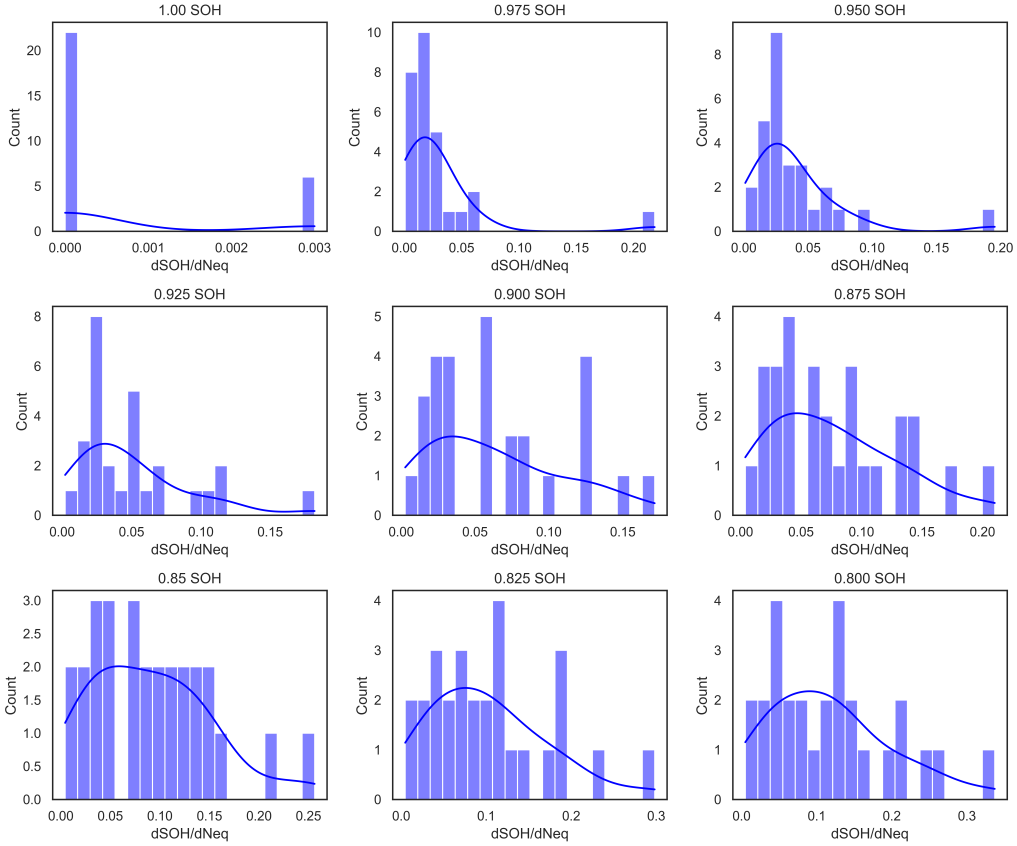

Figure A.1: A histogram showing dSOH/dNeq distribution for all the SOH subsets.

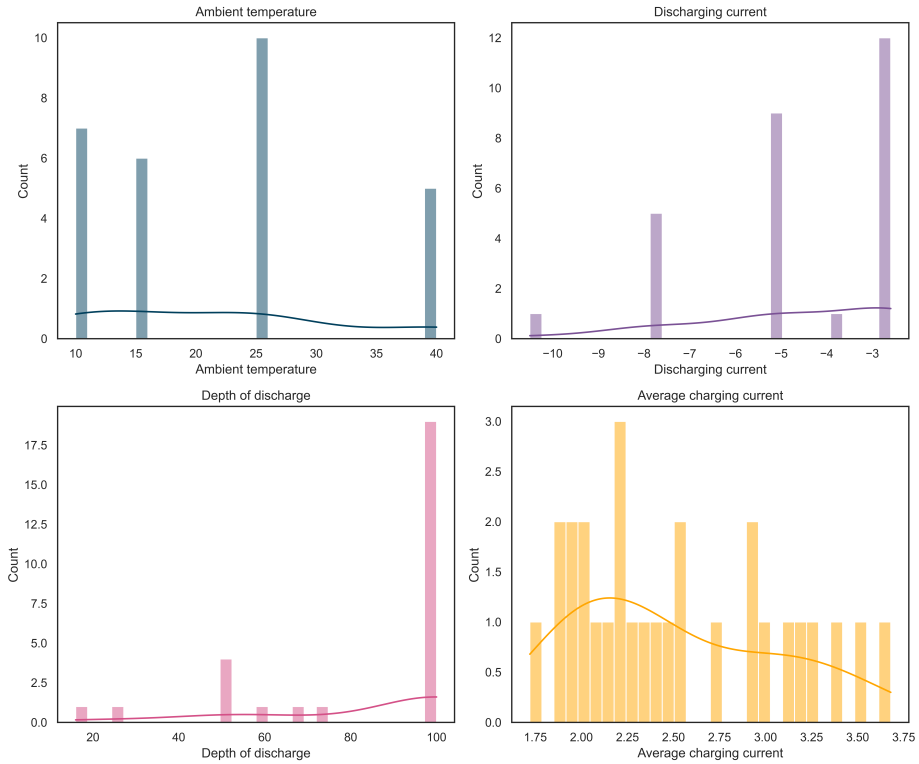

Figure A.2: A sample histogram showing cycling conditions (features) distribution for 0.975 SOH. The distribution is same for remaining SOHs.

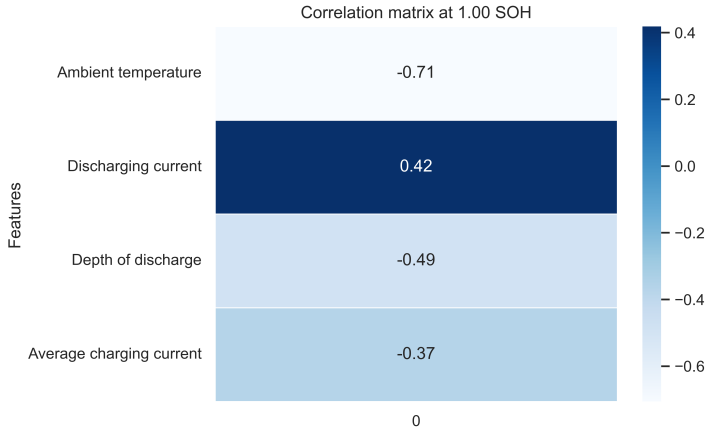

Figure A.3: Spearman's rank correlation coefficient at 1.00 SOH

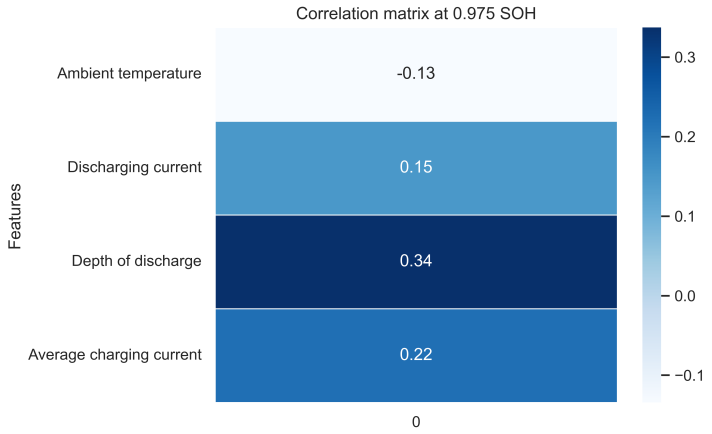

Figure A.4: Spearman's rank correlation coefficient at 0.975 SOH

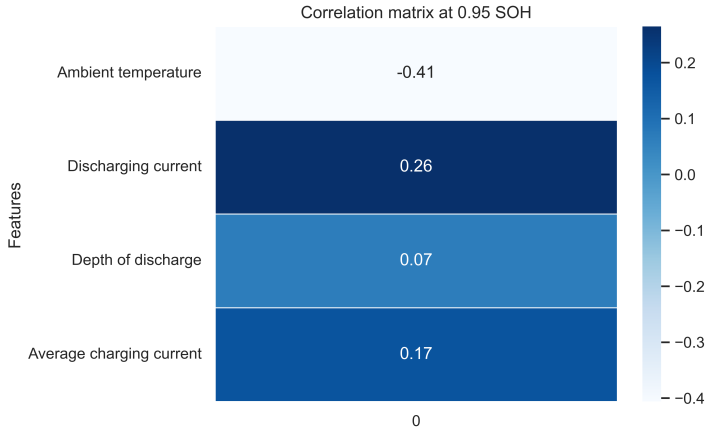

Figure A.5: Spearman's rank correlation coefficient at 0.95 SOH

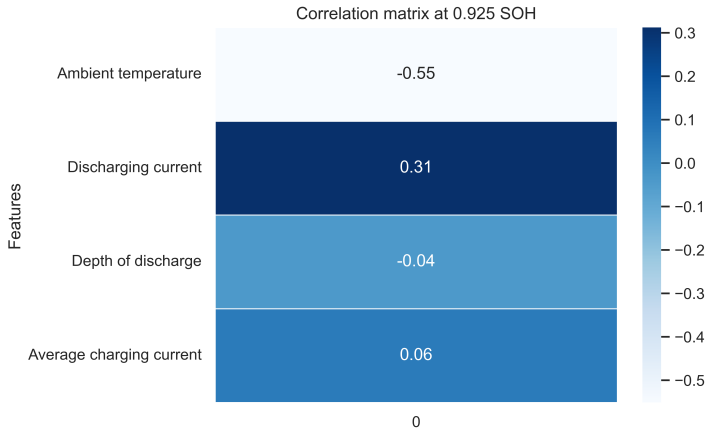

Figure A.6: Spearman's rank correlation coefficient at 0.925 SOH

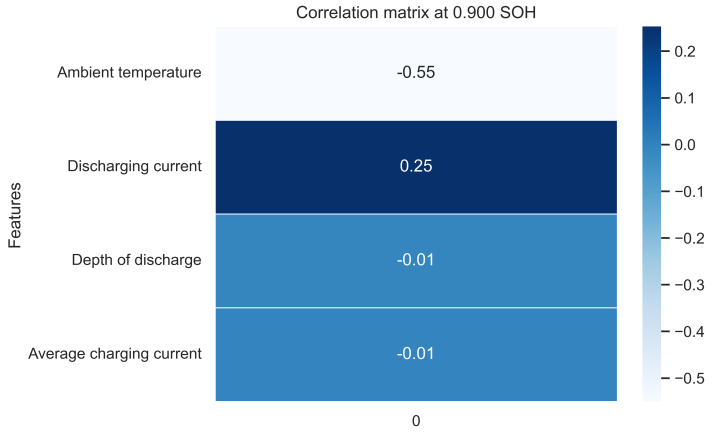

Figure A.7: Spearman's rank correlation coefficient at 0.90 SOH

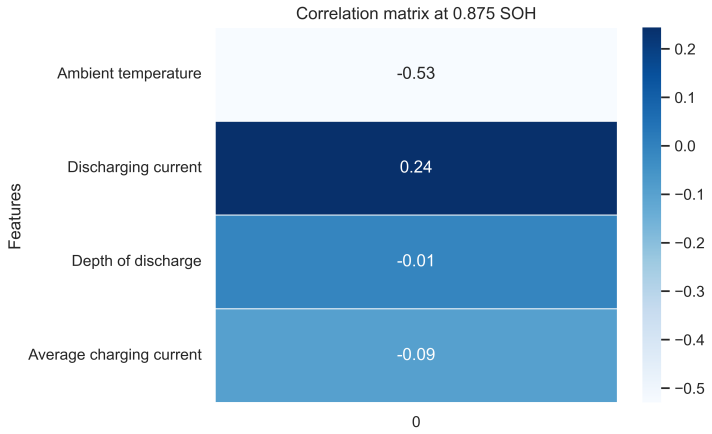

Figure A.8: Spearman's rank correlation coefficient at 0.875 SOH

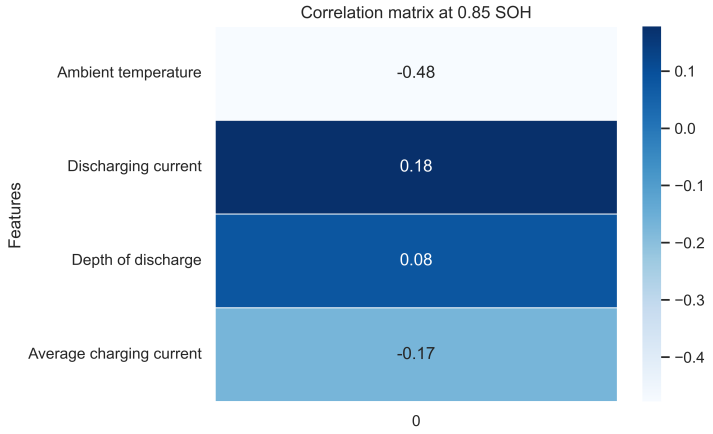

Figure A.9: Spearman's rank correlation coefficient at 0.85 SOH

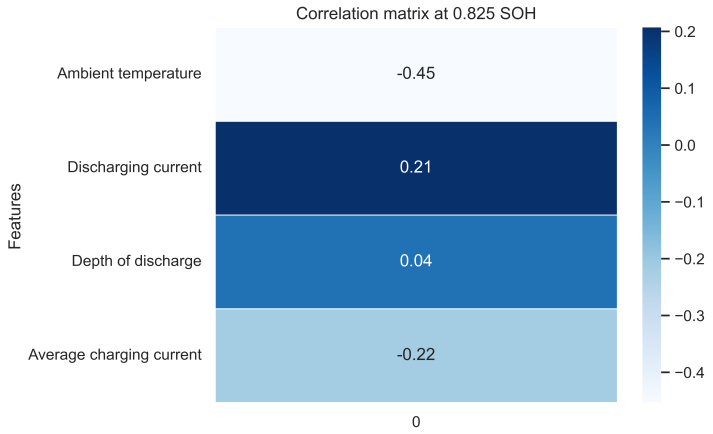

Figure A.10: Spearman's rank correlation coefficient at 0.825 SOH

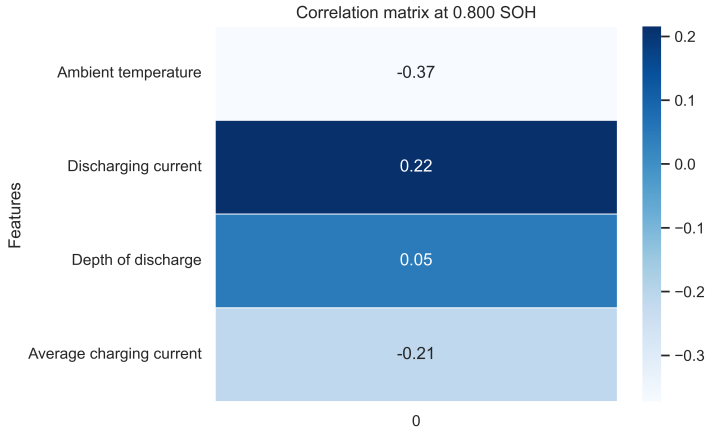

Figure A.11: Spearman's rank correlation coefficient at 0.80 SOH

Table A.3: Compiled evaluation metrics for random forest regression.

Metric\SOH	1	0.975	0.95	0.925	0.9	0.875	0.85	0.825	0.8
Explained Variance Score	0.97	0.18	0.21	0.64	0.76	0.78	0.83	0.83	0.87
Mean Absolute Percentage Error	*N/A*	1.56	1.24	0.61	0.63	0.51	0.49	0.54	0.47
Root Mean Squared Error	0.00	0.04	0.03	0.02	0.02	0.02	0.02	0.03	0.03
R-squared	0.97	0.18	0.21	0.64	0.75	0.77	0.83	0.83	0.87
Mean Absolute Error	0.00	0.02	0.02	0.02	0.02	0.02	0.02	0.02	0.02

Table A.4: Five fold cross validation scores

k-fold/SOH	1	0.975	0.95	0.925	0.9	0.875	0.85	0.825	0.8
k = 1	-0.0012	-0.0384	-0.0355	-0.0325	-0.0347	-0.0308	-0.0344	-0.0352	-0.0452
k = 2	-0.0007	-0.0125	-0.0161	-0.0301	-0.0314	-0.0312	-0.0295	-0.0248	-0.0273
k = 3	-0.0001	-0.0163	-0.0196	-0.0252	-0.0427	-0.0606	-0.0837	-0.1070	-0.1274
k = 4	-0.0001	-0.0177	-0.0216	-0.0267	-0.0223	-0.0212	-0.0300	-0.0382	-0.0433
k = 5	0.0000	-0.0189	-0.0181	-0.0142	-0.0212	-0.0291	-0.0373	-0.0440	-0.0496

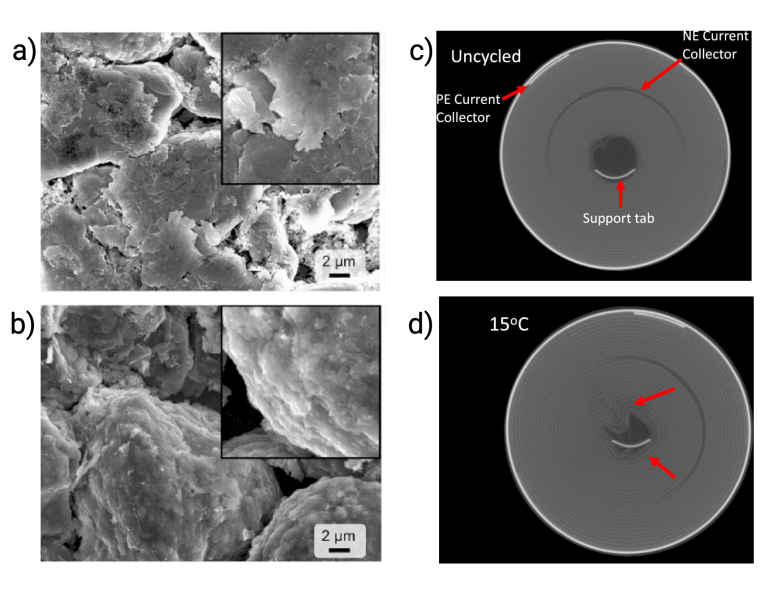

Figure A.12: A comparison of fresh (top) and degraded (bottom) cells due to the effect of temperatures. a) The growth of SEI layer with increase in temperature observed by scanning electron microscopy (SEM) images. Reproduced with permission from ref [11]. Copyright 2014 Elsevier. b) The occurrence of lithium platting at low temperature observed by x-ray computed tomography. Reproduced with permission from ref [9]. Copyright 2023 IOP Publishing.

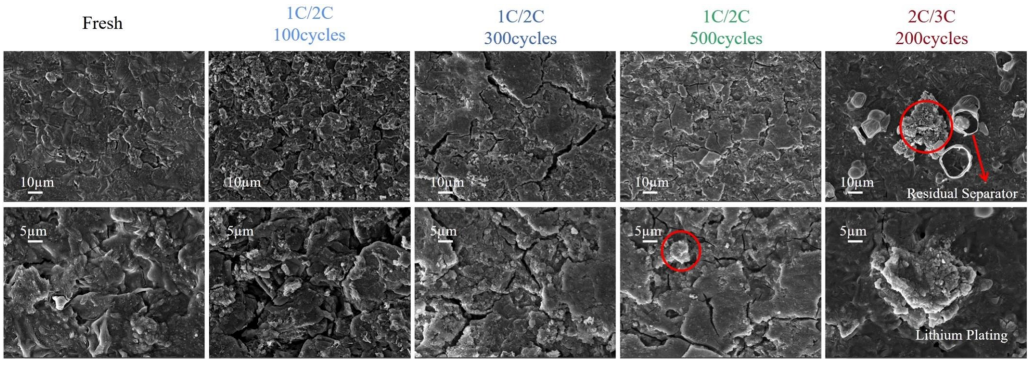

Figure A.13: SEM images showing the early degradation of a cell (lithium platting and particle detachment) with increase in charge/discharge rates. Reproduced with permission from ref [79]. Copyright 2023 Elsevier.

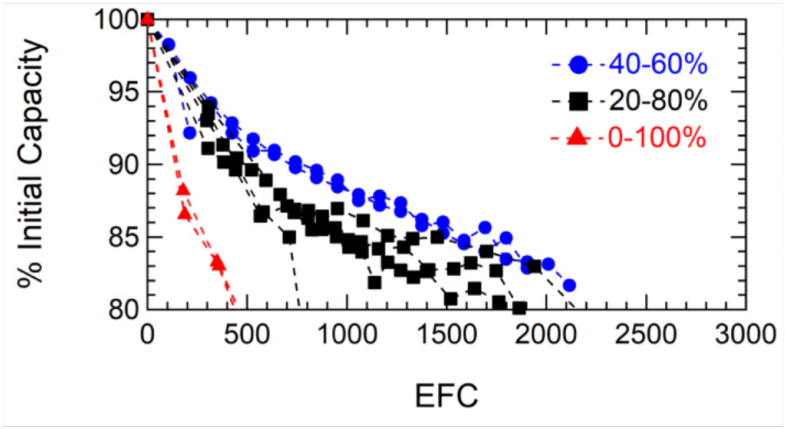

Figure A.14: A plot showing the effect of DoD for NMC 18650 cell at 0.5 C discharge and 25 °C. Reproduced with permission from ref [13]. Copyright 2020 IOP Publishing.

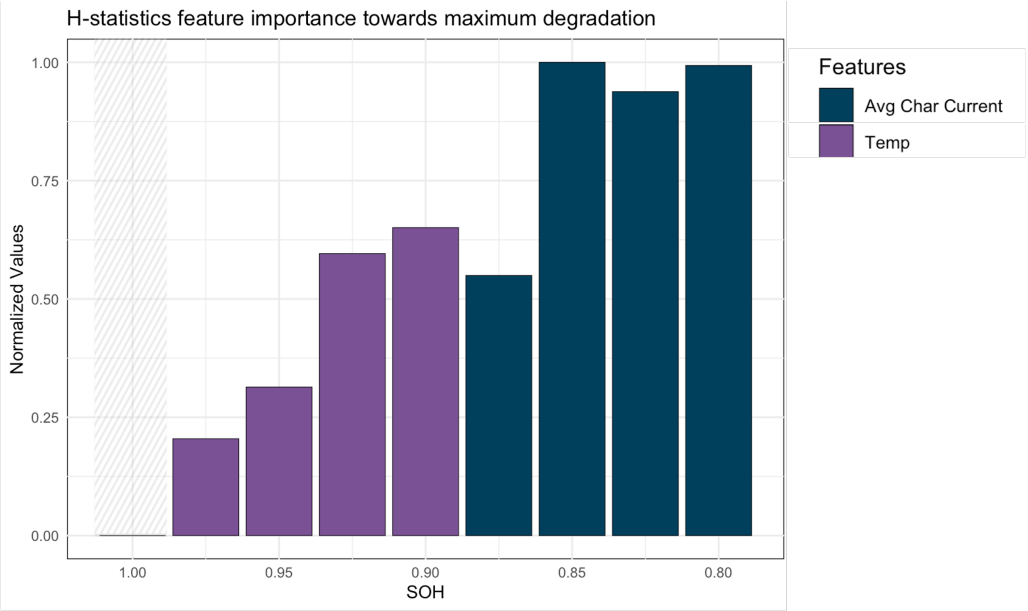

Figure A.15: A bar plot for H-statistics based feature importance.

Data Availability

The dataset used in the current study can be downloaded from the link provided by original authors.

NMC cell 2600 mAh cyclic aging data

Code Availability

The code used for processing and analysis is available at github.

https://github.com/hemantnr/MS-thesis.